electrode arrays (e.g., Chow & Chow, 1997; Chow et al., 2001; Eckmiller, 1997; Eger, Wilms, Eckhorn, & Schanze, 2005; Humayun et al., 1996, 1999, 2003; Peyman et al., 1998; Rizzo & Wyatt, 1997; Schanze, Wilms, Eger, Hesse, & Eckhorn, 2002; Schwahn et al., 2001; Wilms, Eger, Schanze, & Eckhorn, 2003; Zrenner et al., 1997, 1999; Zrenner, 2002).

The sub-retinal devices are implanted between the pigment epithelial layer and the outer layers of the retina. Electrical stimulation with such devices directly activates the overlying retinal tissue, for example the outer plexiform layer and bipolar cells in the case of photoreceptor degeneration. The stimulation parameters can partly be determined by the electronics of the implant, and local stimulation is triggered by the light falling onto a micro-photo-diode (or—transistor) array. Stett, Barth, Weiss, Haemmerle, and Zrenner (2000) have shown in in vitro experiments in normal and degenerated rat retinae, stimulated by multi-electrode arrays, that spatial resolution at retinal level, as determined by ganglion cell recordings, is at least 70 μm corresponding to 1/3° visual angle. Chow and colleagues (2001; Chow et al. 2002) have reported implantation of a passive sub-retinal device (without external energy supply) into the eye of patients, using the method of Peyman (1998). This study was designed to examine biocompatibility of their sub-retinal devices but not their function. After a very short initial phase of diffuse phosphene perception at the site of the device no further light perception was reported by the patients. However, some improvement of still functioning retinal areas, probably due to the release of growth factors induced by the surgery, the result of subthreshold electrical stimulation or the presence of the device itself, have been reported by some of the patients.

Epi-retinal implants are placed from the vitreous side onto the ganglion cell and nerve fiber layer of the retina. In response to visual stimulation through an external image sensor-array, combined with a real-time retina-processor (e.g., see Eckmiller, 1997), the epi-retinal implant evokes action potentials in retinal ganglion cells and their fibers. Finally, both types of implants send visual information in the form of spike patterns of the ganglion cells via the optic nerve to central visual structures.

In recent experiments, the retina of blind patients was electrically stimulated and they reported sensations of light spots in response to focal electrical stimulation of the inner retina (Humayun et al., 1996, 1999, 2003; Rizzo & Wyatt, 1997). These experiments clearly demonstrated the feasibility of generating perception of light patterns in blind people by retinal stimulation. Presently, no final conclusion can be drawn from the first experiments with patients about how close retinal implants meet the below given estimates of minimal requirements for useful artificial vision.

Some principal technical and biophysical problems have been solved for visual prostheses in recent years (Chow & Chow, 1997; Eckmiller, 1997; Hesse, Schanze, Wilms, & Eger, 2000; Humayun, Probst, Juan, McCormick, & Hickingbotham, 1994; Humayun et al., 1996, 1999, 2003; Normann, Maynard, Guillory, & Warren, 1996; Normann, Maynard, Rousche, & Warren, 1999; Rizzo et al., 1999; Schanze et al., 2002; Stett et al., 2000; Wilms et al., 2003; Wyatt & Rizzo, 1996; Zrenner et al., 1997, 1999; Zrenner, 2002). However, one crucial question remains regarding the type of neural responses evoked in the visual cortex by stimulation with retinal implants. To be potentially useful for visual perception, spatial, temporal, and intensity resolutions must be sufficient to discriminate objects in a static environment and to perceive motion in the dynamic scenes of everyday life.

1.2. Minimal requirements for useful artificial vision

Object recognition relies mainly on spatial resolution. A resolution better than 0.5° of visual angle corresponds to a visual acuity of 1/35 where clinically vision testing starts. 0.5° visual angle is therefore the ultimate goal in the development of retina implants. 2° resolution will lead to *improvement of performance in daily life*, like the recognition of objects that are important for taking meals, for washing, and dressing. Finally, 10° resolution might be sufficient for *mobility and orientation*, allowing subjects to perceive the presence of large objects and their movement directions (e.g., Legge, Ahn, Klitz, & Luebker, 1997). However, gaining at least some improvement of performance in daily life would be highly valuable for blind people and even regaining some mobility and orientation could improve their quality of life considerably. In normal visual processing, spatial resolution can be estimated at any stage of the visual system from the size of the classical receptive fields (CRFs) of its neurons. Inversely, spatial resolution can also be estimated from the spread of neural activation in the primary visual cortex in response to focal retinal stimulation as is done with small visual stimuli and electrical impulses in this investigation.

Minimal requirements for useful artificial vision can be estimated by psychophysical methods (e.g., Cha, Horch, & Normann, 1992a; Legge et al., 1997; Sommerhalder et al., 2003). Near perfect reading at central retinal projection sites requires at least 300 sampling points of the text to be read within about 5° retinal eccentricity. If safe navigation in dynamic out-door environments is also required, stimulation should include eccentricities of 10–15° (Cha et al., 1992a; Geruschat, Turano, & Stahl, 1998) where spatial resolution for navigational purposes can be lower. About 200 additional sampling points are sufficient within this outer "navigational belt." The number of required sampling points and their spatial distance define the required number and spacing of stimulation electrodes in a retinal implant. With the above psychophysical estimates, a total of about 500 electrodes would be necessary for useful artificial vision.

1.3. Intensity and time resolution

Retinal ganglion cells transmit retinal visual information to higher visual centers—in normal vision and with retinal

implants (independent of epi- or sub-retinal stimulation). Single ganglion cells code, to a first approximation, temporal sequences of local contrasts (intensities) within their receptive fields by spike rate modulations, based on the synaptic preprocessing in the network of inner and outer retinal neurons. This means that the coding resolutions of intensity/contrast and time are intimately related. As the maximal spike rate of a ganglion cell is limited, the number of different successive intensity values that can be transmitted in the absence of noise in terms of Shannon information (Eckhorn & Pöpel, 1975, 1981; Eckhorn, Grüsser, Kröller, Pellnitz, & Pöpel, 1976; Eger et al., 2005; Rieke, Warland, de Ruyter van Steveninck, & Bialek, 1998; Shannon, 1948) is mainly determined by the amount of time available for transmitting a single contrast value. For example, if a neuron can discharge maximally 32 action potentials during 333 ms (average duration of ocular fixation) it can theoretically code one out of 32 different intensity values within each of the 3 fixation intervals per second (or 5 bit of information in 333 ms which equals 15 bit/s). This resolution seems sufficient for most visual fixation tasks in which spatial details and high resolution of contrasts play a prominent role. If, on the other hand, a pedestrian wants to cross a road in heavy traffic, local contrast resolution is of minor importance, and may be reduced to only 4 different values (resembling 2 bit). However, in such a situation temporal resolution is of vital importance, and needs to be markedly increased to enable effective coding. Our example neuron can at best signal 2 bit by 1–4 spikes per time window of 41.7 ms. Hence, within one second it can transmit 24 times 2 bit equal to 48 bit/s (again assuming the absence of noise). This example demonstrates that a reduction in intensity resolution (from 5 bit to 2 bit per sample or frame) results in a concomitant increase of temporal resolution (from 3 to 24 samples per second) and an overall increase in the rate of information from 15 bit/s to 48 bit/s. It is important to keep in mind that the signals carrying the information are in first approximation spike densities (rates) that can be read out by the succeeding stages of the visual system at quite different speeds (integration window) with the consequence that an increase in temporal resolution reduces the contrast resolution while overall rates of information can increase. It is probable that the visual centers adaptively change the temporal resolution (Agmon-Snir & Segev, 1993) according to the current visual situation which, in turn, affects the available contrast resolution. Retina implants have to generate spike density coding so that the visual centers can use their flexible strategy in which the trade-off between intensity and time resolution is continuously optimized.

1.4. Estimates of spatial and temporal resolutions from anesthetized cats

Before extensive investigations of perceptual resolution with retina implants are carried out in blind humans, we considered it ethically appropriate to test and optimize stimulation with retinal implants in animal models. Based on the existing broad knowledge about the visual systems of cats (e.g., Gilbert, 1993; Hubel & Wiesel, 1962; Tusa, Palmer, & Rosenquist, 1978; overview: Orban, 1984), we used this species to estimate the achievable resolution in human visual perception with sub- and epi-retinal implants. Most importantly, for identical visual stimuli, human visual perception has been shown to correlate with the receptive field properties of visual cortical neurons in lightly anaesthetized monkeys and cats. Correlations were demonstrated for a variety of perceptual and neural thresholds of visual cortical neurons, including those for luminance and color contrast, flicker frequency, movement direction, and velocity (e.g., Gilbert & Wiesel, 1990; Grind van de, Grüsser, & Lunkenheimer, 1973; Heydt von der & Peterhans, 1989; Knierim & van Essen, 1992; Salzman, Britten, & Newsome, 1990; Wachtler, Sejnowski, & Albright, 2003; overview: Tovee, 1996). From these observations and retinal lesion experiments in primary visual cortex, one can conclude that perception of visual details requires the activation of neurons in this area (e.g., Darian-Smith & Gilbert, 1995). From the time course of their activations by a focal retinal stimulus impulse estimates of perceptual temporal resolution should be possible (Dinse & Krüger, 1994; Grüsser & Creutzfeld, 1957; Rager & Singer, 1998; review in: Bullier, Hupe, James, & Girard, 2001). In addition, the spatial extent of the cortical activations to such stimuli can give conservative estimates of spatial visual resolution. This is possible because the lower visual cortical areas (particularly area 17/V1) are retinotopically well organized so that spatial profiles of cortical activations can directly be related to retinal and visual space (Adams & Horton, 2003; Angelucci, Levitt, Walton, Hupé, & Bullier, 2002; Tusa et al., 1978). These measures were verified in our investigation by light stimulation of the retina before implantation of electrodes combined with recordings of cortical activities from the identical positions used during electrical stimulation.

2. Methods

Stimulation experiments with cortical electrode recordings were performed in 9 adult cats in 13 sessions, and with optical cortical recordings in 4 adult cats (3–5 kg). All experiments were done in accordance to the guidelines of the European Communities Council Directive (86/609/EEC) and were approved by official German Animal Care and Use Committees following the NIH Principles of Laboratory Animal Care (Publication 86–23, revised 1985) and the ARVO guidelines.

2.1. Preparations

Preparations for cortical microelectrode and optical recordings were similar as reported in detail elsewhere (Kisvarday, Buzas, & Eysel, 2001; Schanze et al., 2002; Wilms et al., 2003). Briefly, adult cats received an initial anesthesia with ketamine hydrochloride (Ketanest, 10 mg/kg) and xylazine hydrochloride (Rompun, 1 mg/kg) that was about 2 h later maintained by a mixture of N_2O/O_2 (70%/30%) and halothane (0.3–0.8%, optical imaging experiments) or isofluorane (0.5–1.5%, microelectrode recording experiments) using oro-tracheal intubation for artificial respiration. Eye movements were minimized by i.v. infusion of alcuronium chloride (0.1 mg/(kg h)). End-tidal CO_2 (3–4%), blood pressure (100–140 mmHg), and body temperature (38–39 °C) were monitored continuously.

Semi-chronic preparations for cortical microelectrode recordings were made with initial surgery and anesthesia (induced and prolonged) corresponding to the acute preparations except for the use of oro-tracheal intubation instead of tracheal cannulation for artificial ventilation. For head fixation and the attachment of a recording chamber over the craniotomy at V1/V2 positions, two bolts were implanted in cavities of the forehead. In some cases, an optically controlled laser coagulation of the peripheral retina was performed to reduce the risk of a retinal detachment due to vitreal tractions after insertion of stimulation electrodes.

The refraction of the non-implanted eye was corrected for the viewing distance of the visual stimulation screen at 1.3 m in front of the eyes.

2.2. Insertion of electrodes for epi-retinal stimulation

After lateral canthotomy at one eye the conjunctiva was incised (~1 mm), and a sclerostomy performed behind the limbus, sufficient for insertion of the epi-retinal fibre-microelectrode stimulation arrays. Alternatively, epi-retinal foil electrode arrays (polyimide–platinum thin-film electrodes) were implanted after lensectomy and vitrectomy through corneal incisions and placed on the retinal surface adjacent to the fovea centralis. The position of the foil electrode array was stabilized with Perfluordecalin.

Insertion of fiber- and thin-film electrodes for epi-retinal stimulation was made as described in detail by Schanze et al. (2002). Briefly, the fiber electrodes (80 μm shaft diameter; Reitböck, 1983) were ground to expose a metal (PtW) cone tip (~20 μm diameter, ~30 μm height) allowing safe charge delivery of up to 20 nC per impulse. The fiber electrodes were axially positioned singly under visual control using a computer driven, adapted fiber electrode manipulator (Eckhorn & Thomas, 1993; 1 mm concentric bundle of 3 or 7 electrode guide tubes) attached to another specially developed manipulator with 11 degrees of freedom (NeuroPhysics, University of Marburg). This system allowed fast, precise, and flexible electrode positioning through the small scleral opening (1.1 mm). In several experiments (see Section 3), thin-film arrays (platinum islands of 100 μm diameter on polyimide) were used for stimulation (Stieglitz, Beutel, Schuettler, & Meyer, 2000). For low energy activation, the electrodes were brought in direct contact with the inner limiting membrane under visual guidance. To control correct positioning, multiple unit activity (MUA) of retinal ganglion cell fibers was recorded via the stimulation electrodes.

2.3. Insertion of electrodes for sub-retinal stimulation

For a safe introduction of sub-retinal implants, the approach with access through the vitreous body of the eye (ab interno) as published by Peyman et al. (1998) as well as Sachs et al. (1999) was used. In short, a modified pars-plana-vitrectomy approach was used in the eyes after pupil dilation with atropine 1%. The high reflectivity of the tapetum lucidum required no endoillumination, thereby enabling two port vitrectomy. Two sclerotomies were made 6.0 mm posterior to the limbus. After partial vitrectomy between sclerotomy and area centralis, a 31 gauge cannula (Visitec, Sarasota, FL) was used to create a localized retinal bleb by injecting a small amount of balanced salt solution; the bleb was enlarged by injecting Healon® (Pharmacia, Stockholm, Sweden). A 2.5-mm retinotomy was then made circumferentially at the temporal portion on the bleb. The foil was introduced into the vitreous cavity with an intravitreal end-gripping forceps. After the foil was inserted through the retinotomy into the sub-retinal space, it was forwarded about 1 mm outside the created bleb under the retina near the area centralis (Volker et al., 2006).

The stimulation array consisted of thin-film platinum electrodes mounted on a flexible polyimide foil (Fraunhofer Instit. Biomed. Engin., St. Ingbert, Germany; model RS8-50; Stieglitz et al., 2000). The flexible foil strip was made of 50 μm thin polyimide with 8 substrate-integrated, insulated golden connection lanes terminating in a 2 by 4 array at the end of the strip with an even spacing of 330 μm (see Fig. 4). Rectangular openings (100 μm × 100 μm) in the insulation layer at the terminals of the lanes define the size of the stimulation electrodes. The gold electrodes were covered with a thin layer of platinum to enhance the safe charge injection capacity. At the other end of the foil strip a plug was soldered to the contact pads to allow connection with the computer controlled stimulator device (STG 1008, Multi Channel Systems, Reutlingen, Germany). At the end of each experimental session, sclera and conjunctiva were sutured, all wounds topically medicated, and infections were prevented by injections of penicillin (i.m.). The animals recovered rapidly so that after a few weeks repetitive investigations of the same eye could be performed (Gekeler et al., 2004).

2.4. Stimulation and recording

2.4.1. Epi- and sub-retinal stimulation

For epi-retinal stimulation generally rectangular constant current impulses were applied (~200–250 μs duration per polarity; ±1–150 μA). They consisted of charge balanced pairs of a negative and positive phase (cathodic first; controlled constant current sources developed by T. Schanze, manufactured by M. Eger, Uni-Marburg, Physics Department). In some cases, bursts of 2–10 such impulse-pairs were applied (0.4–2.0 ms burst duration). In optical imaging experiments, trains of biphasic stimuli were also applied (see below). For sub-retinal stimulation (see, e.g., Fig. 1B) biphasic impulses (anodic first) with amplitudes up to ±50 μA were applied against a ground electrode. Stimulus duration was 0.5–1.0 ms per phase applied at intervals of ISI = 305 ms.

Before optical imaging the visual cortex, the function of the retinal implant was tested by electrode recordings from the optic tract, made with a concentric bipolar tungsten electrode (SNEX-100, Rhodes Medical, Woodland Hills, CA, USA). Penetrations were performed at Horsley–Clarke coordinates A14/L2 just behind the optic chiasm. For positioning of the recording electrode at the correct depth, recordings were made during 1 Hz stroboscopic light flash stimulation. The optimal position of the electrode was reached, when the maximal flash evoked field potentials were obtained and the electrode was fixed at this position using dental cement. To compare the visual response amplitude to the electrically evoked responses and to judge the relative efficacy of stimulation at the different electrodes in the epi-retinal array, short, single biphasic electrical stimuli (4–78 μA; balanced current; waveform: 250 μs negative; 250 μs off; 250 μs positive) were delivered at 1 Hz via all single electrodes of the implant against ground (electrode No. 19, see Fig. 4A).

With sub-retinal stimulation, optic tract responses were evoked by electrical stimulation (±50 μA, biphasic current pulses as described above). Electrodes 1, 2, 3, and 4, respectively, served as different electrodes, the combined electrodes 5–8 of the implant were used as ground. The small field potentials were averaged from 128 repetitive stimuli (see Fig. 4B).

Cortical electrode recordings were made in area 17 and 18 (Horsley–Clarke coordinates: A2-P7, L0.5-L3) with up to 16 microelectrodes. For technical details, see Wilms et al. (2003). Briefly, linear arrays of fiber electrodes (2–3 M at 1 kHz) were used and signals were extracted in real time from each electrode's broad band recording: single unit spike activity (SUA), multiple unit spike activity (MUA), and local field potentials (LFP, 1 or 10–140 Hz). SUA was captured as events whereas the continuous amplitude signals MUA and LFP were sampled at 500 Hz. Alternatively, the broad band raw signals (1–4000 Hz) were sampled at 20 kHz for off-line filtering to SUA, MUA, and LFP, enabling a better rejection of the stimulation artifacts (Schanze et al., 2002). All signals were stored on a hard disk for off-line data evaluations.

2.5. Receptive fields

The receptive fields (RF) of the recorded cortical neurons were determined qualitatively using a hand held projector and quantitatively with computer generated stimuli presented on a monitor (100 Hz frame rate, high contrast), composed of random m-sequences (multifocal RF-measurements, Sutter, 2001). After simultaneous on-line mapping of all cortical RFs, the positions of the retinal RFs were determined by the same MUA recording method. The tip positions of the stimulation electrodes and retinal landmarks (blind spot and area centralis) were marked by rear projection onto a tangent screen using a custom designed laser projection

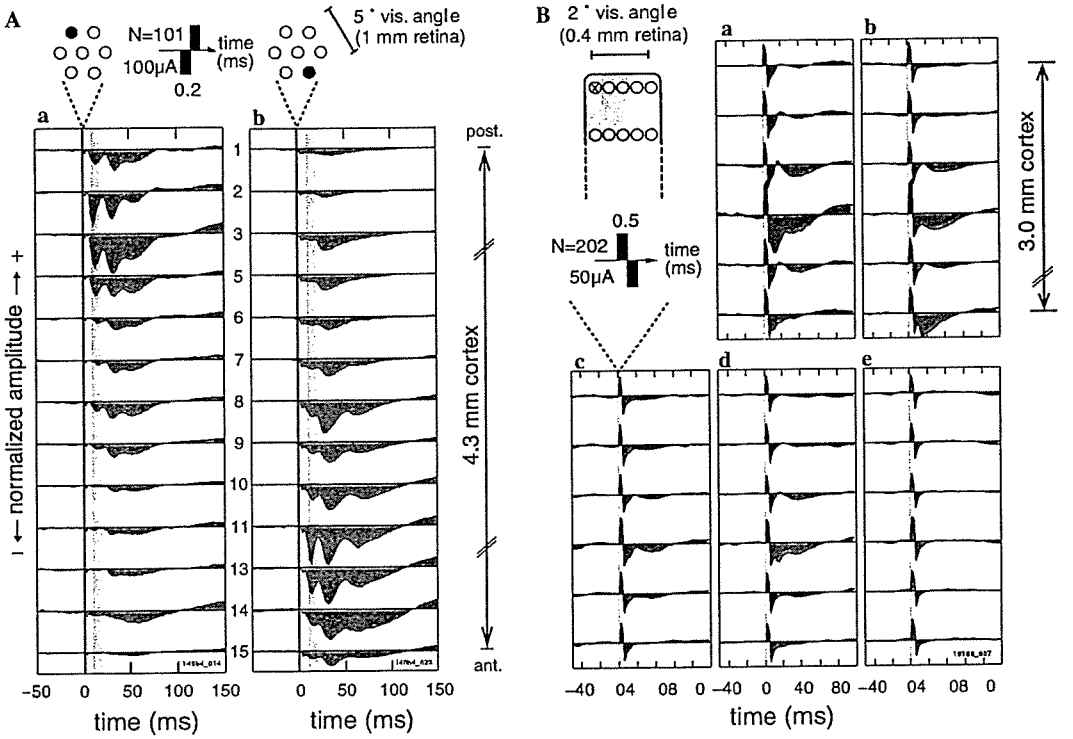

Fig. 1. Time courses of cortical population activities (LFP) in response to single-site retinal stimulation. (A) Responses to epi-retinal impulse stimulation ($N = 101$ identical stimulus repetitions) recorded simultaneously at 13 different locations by a linear electrode array (0.3 mm equi-distant pitch). The 10 ms gray band marks the primary cortical signals in direct response to the afferent stimulus evoked population spike. (B) Responses to sub-retinal impulse stimulation ($N = 202$) at five retinal electrode positions (a–e) recorded simultaneously at six different cortical locations by a linear electrode array (0.5 mm equi-distant pitch). The insets on top of column (A) and (B) depict the geometry of retinal stimulation sites and the time courses of stimulation current impulses with durations of 0.2 ms (A) and 0.5 ms (B). The retinotopic correspondence between retinal stimulation and cortical recording sites can be derived from the responses. The higher the response amplitudes the better the correspondence. This means for (Aa): best correspondence with electrode 3. For (B) the stimulation electrodes, used for the data in (Ba–e), are marked by gray background. Correspondence: electrodes used for (Ba) and (Bb): upper row left and right, respectively; for (Bc): lower row left and for (Be): lower row gray field right. Best retinotopic correspondence for data in (Ba and c–e) with electrode 4 (counted from top of each panel), for data in (Bb): el. 4 and 6.

system. Retinal electrode positions were corrected until cortical and retinal RFs sufficiently overlapped.

2.6. Optical imaging of intrinsic signals

Optical imaging of intrinsic signals was carried out using the Imager 2001 and the data acquisition software VDAQ-NT (both Optical Imaging, Germantown, NY, USA) as reported previously (Kisvarday et al., 2001). Briefly, a bilateral craniotomy was made between Horsley–Clarke coordinates AP −6 and +12 and LM +0.5 and +7 to expose the central visual representation of visual areas 17 and 18. A round stainless steel chamber (31 mm diameter) was mounted over the exposed cortical region, the dura-mater was removed and the chamber filled with silicone oil (50 cSt viscosity, Aldrich, Milwaukee, WI, USA) and sealed with a round cover-glass. During data acquisition, the camera (two SMC Pentax lenses, 1:1.2, $f = 50$ mm, arranged in a "tandem" manner, Ratzlaff & Grinvald, 1991) was focused 650–750 µm below the cortical surface and the cortex was illuminated with 609 ± 5 nm light (filter: Omega Optical, Brattleboro, VT). Imaging was carried out separately for visual stimuli through the non-operated control eye and for electrical activation via the implanted retinal electrodes.

2.6.1. Optical imaging using visual stimulation

Visuotopic mapping was performed using test stimuli presented on a video screen (SONY, Pencoed, UK) in 120 Hz non-interlaced mode 28.5 cm in front of the cats' eyes using the VSG Series 3 stimulus generator system (Cambridge Research Systems, Rochester, UK). The test stimulus consisted of a narrow horizontal slit (0.5–3 deg width and 40 deg length) encompassing a high-contrast vertical grating (50% duty cycle) 0.6–1 cyc/deg spatial frequency moving forth and back at 1–2 Hz. Stimuli were presented at visual field elevations encompassing the central 10 degrees and displayed in a random sequence. Each data acquisition period (4.5 s during which the stimulus grating moved) was preceded by an inter-stimulus interval of 10 s when the animals viewed a blank screen (average luminance of the stimulus grating).

2.6.2. Optical imaging using electrical stimuli

For obtaining intrinsic signal images of cortical activation due to electrical stimuli of the implanted electrodes a data acquisition paradigm similar to that of the visual stimulation was used (4.5 s duration, 10 s inter-stimulus interval). During a single data acquisition period, 9 trains of current pulses were applied (250 ms train duration with 250 ms intervals). Each train consisted of a barrage of 0.75 ms bipolar current pulses (±4–78 µA, 250 µs negative, 250 µs baseline, 250 µs positive repeated at 100 Hz).

2.6.3. Analysis of the optical images

For data analysis, single condition maps (SCMs, c.f. Bonhoeffer & Grinvald, 1996) were calculated by summing the images associated to a particular stimulus condition using the Winmix software (Optical Imaging, Germantown, NY, USA). The SCMs were filtered with a Laplace filter (high-pass: 50 pixels, 1064 µm) followed by a boxcar filter (low-pass: 5 pixels, 106 µm).

2.7. Data analysis

2.7.1. Cortical electrode recordings

The population signals, MUA and LFP, were simultaneously available at all functioning cortex electrodes (~80%) and good SUA (at ~25% electrodes) were detected after the initial electrode positioning in the upper layers without any search for large spikes. Responses to identical stimulus repetitions were averaged with respect to stimulus onset to obtain peri-stimulus time histograms (PSTHs) from which we determined the cortical response thresholds, delays, and strengths to retinal stimulation. These measures were based on average response power after scaling to the corresponding pre-stimulus values. In addition, LFP and MUA response power were plotted in relation to stimulation strength to estimate thresholds.

2.7.2. Optical recordings of intrinsic cortical signals

The optical recordings of intrinsic signals evoked by electrical retinal stimulation revealed two-dimensional activity patterns in a cortical area of 6 × 8 mm. The grey values of the respective maps coded the activity on a 0–255 gray scale with 0 (black) representing maximal, and 255 (white) minimal activation. The peaks in the spatial pattern of activation were used for estimation of spatial resolution.

Spatial resolution was estimated from the spread of cortical activation in response to a focal retinal stimulus, defined as the retino-cortical point spread function. It was either derived by sampling from linear electrode arrays with 0.3 or 0.5 mm spacing (7 or 16 microelectrodes) or by measuring the spread of activation with optical imaging. For electrode recordings, the spatial distribution of response amplitudes was fitted by a Gaussian function and its full width at half height was taken as the magnitude of the cortical point spread. In addition to this, the same procedure was used to determine the cortical point spread to visual retinal stimulation. In this case, a small focal flash was shown at the same retinal location in the corresponding location of the non-implanted eye (results not shown).

Most response profiles were measured with cortical microelectrode recordings between 4° and 9° retinal eccentricity. The remaining optical recordings were from 0° to 15° eccentricity. To compare these different profiles, we took the magnification factor from the cat visual cortical maps (thoroughly measured by Tusa et al., 1978 & Tusa et al., Tusa, Rosenquist, & Palmer, 1979) at the recording site of every single cortical activation profile. For comparison, we took the individual magnification factors for normalization to a reference eccentricity of 2° visual angle. We chose this reference at 2° because the retina implants in progress will probably span a total visual angle of about ±4°, so that 2° eccentricity is just half way out from the center. The response profiles measured with cortical electrodes were recorded at eccentricities between 4° and 9° in the lower visual field where the magnification factor in cat does not change very much with eccentricity. The fewer optical recordings were made at eccentricities between 0° and 15°. This normalization seems appropriate when we assume that the size of a retinal patch, activated by a single electrode, is independent of eccentricity because the spread of the electrical stimulation field will not change with eccentricity. Therefore the corresponding activation patch in area 17 decreases with increasing eccentricity, and this effect has been normalized by us.

Estimates of resolutions for contrast and time were obtained with two methods. In the "direct approach," the effective duration and variance of averaged excitatory cortical MUA and LFP activations were related to temporal and amplitude resolutions, respectively. The number of discriminable amplitudes was quantified by the difference between average post- and pre-stimulus amplitudes, and divided by the post-stimulus variance. In the "indirect approach," the rate of transinformation T′ (in bit/s) was used (e.g., Eckhorn & Pöpel, 1975; Eger et al., 2005; Shannon, 1948). It determines the amount of information transmitted from a retinal stimulus electrode to a cortical recording site. 1 bit/s here means that two different stimuli can be distinguished by an ideal observer on the basis of a single observation period of 1 s duration. If, for example, 20 bit/s are transmitted from a retinal stimulation electrode to a cortical recording site (a realistic example), a series of twenty 2-level discriminations (e.g., black/white) are safely transmitted during one second (or 5 consecutively transmitted values per second at a resolution of $2^4 = 16$ different levels; e.g., local contrast values, which also gives 5 × 4 bit = 20 bit/s). Hence, temporal and intensity resolutions are inversely correlated, the higher the temporal the lower the intensity resolution. The Shannon information measure has the advantage that the actual noise level is taken into account so that potential resolutions can be estimated quantitatively for single responses without averaging.

3. Results

3.1. Spatial activation profiles in visual cortex

3.1.1. Microelectrode recordings in visual cortex

The cortical responses evoked by single retinal impulses show different time courses (e.g., Figs. 1A, a and b), depending on the recording location relative to the retinal stimulation site. These differences in time course are, in essence, a sign of fast dynamic changes in the spatial activation profiles. We measured the spatial width of these profiles to estimate the potential spatial resolution obtainable with retina implants. The narrowest distribution is generally present at the first afferent cortical activations (Fig. 1A, gray time slices). One millimeter difference in epi-retinal stimulus location causes in this example a cortical offset in the maximal primary response of ~3 mm (Figs. 1A, a vs. b). The later (secondary) response components display a broader distribution.

The spatial activation profiles (retino-cortical point spread) to epi-retinal stimulation have almost equally often a single (Fig. 2A) or a double peak (Fig. 2B). It can also be noticed that the width of the activation increases slightly with stimulation current (Figs. 2A and B), probably due to an increase in the number of recruited ganglion cells and the related broader and stronger activation of the cortex. A coarse estimate of the full width at half height (FWHH) obtained was 1.0 mm (Fig. 2A; stimulation: each phase 0.2 ms, negative first, 24 μA), 2.7 mm (2B; stimulation: each phase 0.2 ms, negative first, 25 μA) and 1.7 mm (2C; stimulation: each phase 0.5 ms, positive first, 50 μA). For a better comparison of these values, obtained at different retinal eccentricities, we normalized these FWHH values to an eccentricity of 2° visual angle by using the cortical magnification factors corresponding to each of our cortical recording locations (Tusa et al., 1978; Tusa et al., 1979). Normalization resulted in 1.4° (A), 3.8° (B), and 2.4° (C) of visual angle, respectively (see also Section 4).

3.1.2. Optical recordings in visual cortex

Optical recordings revealed results that corresponded well to the microelectrode recordings. While the fast response components could not be monitored separately because of the relatively low temporal resolution of the optical signals, the compound signals of optical recordings revealed activation profiles similar to the late components of the microelectrode recordings. This is demonstrated in Fig. 3 showing different cortical activation profiles in response to different single site retinal stimuli (visual stimulation (Fig. 3A), as well as epi- (Fig. 3B), and sub-retinal (Fig. 3C) electrical stimulation). In line with the

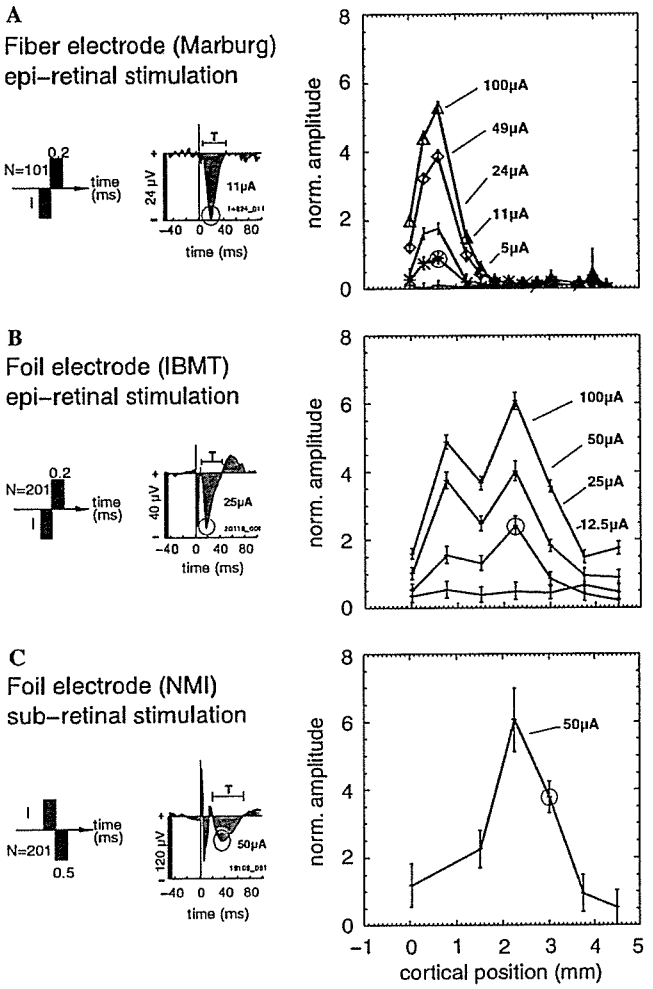

Fig. 2. Spatial cortical activation profiles (right panels) recorded with microelectrodes in response to para-centrally applied single retinal stimulation impulses of different currents I. The normalized amplitudes of the responses for deriving the spatial profiles were taken from the maxima of the first cortical response component after the stimulation artifact (indicated by circles in middle panels, showing example time courses of averaged LFPs at the indicated stimulation currents I; delays of maxima 20–30 ms. T denotes the duration of the first cortical response component). (A) Epi-retinal stimulation with cone electrodes. (B) Epi-retinal stimulation with single electrode of foil array (manufactured by IBMT St. Ingbert, Germany). (C) Sub-retinal stimulation with foil electrode array (manufactured by NMI, Tübingen, Germany). Left panels: time courses of the stimulus current I; number at first impulse indicates its duration in ms, *N* denotes the number of identical stimulus repetitions used for averaging the responses (examples shown in middle panels).

retinotopic organisation of the visual cortex (Tusa et al., 1978, 1979), the cortical activation was localized more posterior when the stimulation was located at lower positions in the retina and moved progressively towards anterior for stimulation sites at upper retinal locations. For a semi-quantitative analysis of the cortical activity, two-dimensional activation profiles were computed on the basis of the gray scale values of the images (Figs. 3B and C). From such data the width of the distributions and their offsets with changes in retinal stimulus location were estimated. A shift of the stimulus by 1.5 mm on the retina led to a shift of the maximum of cortical activation by 3.72 mm (left and rightmost panels in Fig. 3B). The full width at half height (FWHH) of the activity modulation in space was on average 1.78 mm. This FWHH is taken as a measure to estimate the possible spatial resolution (possible discrimination of two adjacent activity profiles) at a given eccentricity along the antero-posterior axis in visual area 18. We have calculated this resolution for the chosen retinal reference eccentricity of 2° (see Section 2: spatial resolution) where 1.78 mm in the visual cortex corresponds to about 2.5° visual angle (Tusa et al., 1979). For these measurements stimulation currents were ±150 µA (250 µs duration of each phase was used for epi-retinal stimuli; s. Fig. 3B) and ±50 µA for the sub-retinal stimuli (1 ms each phase; s. Fig. 3C).

Sub-retinal stimulation and optical recordings revealed similar results as obtained with epi-retinal stimulation. The examples in Fig. 3C show optically recorded activations in response to impulses applied to two different retinal electrodes 0.33 mm apart. They are clearly different in their cortical extent and position of the optical signals. This is demonstrated by the one-dimensional profiles in Fig. 3C. With a 0.33 mm shift of retinal stimulation in the immediate vicinity of the area centralis, the maximum of the cortical signal moves about 1.75 mm on the visual cortical surface. From the 2-D distribution of the activity profiles the spatial extent of activation was measured as FWHH in the same way as for the epi-retinal stimulation. The average value of 1.79 mm FWHH corresponds to approximately 2.5° visual angle at the reference retinal eccentricity of 2° (see Section 2) along the antero-posterior axis in cat visual area 18. This spatial resolution of the optical imaging signal is equivalent to that obtained with epi-retinal stimulation.

Table 1 gives an overview of the estimated spatial resolutions obtained with epi- and sub-retinal stimulation assessed with cortical microelecrode and optical recordings. Resolutions obtained with microelectrode recordings were about a factor of two higher than those with optical recordings. While we measured the highest resolutions (0.68°) with cone-shaped three-dimensional electrodes and epi-retinal stimulation, best results with flat two-dimensional film electrodes (0.9°) were obtained with sub-retinal stimulation.

3.2. Temporal properties of the retino-cortical pathway with electrical activations

Temporal properties of the retino-cortical pathway were analyzed with microelectrode recordings of single and multiple unit spikes (MUA) as well as local field potentials (LFP).

3.2.1. Spike activation patterns of retinal ganglion cells

Spike patterns of microelectrode recordings from the optic tract and retinal stimulation by thin-film arrays were

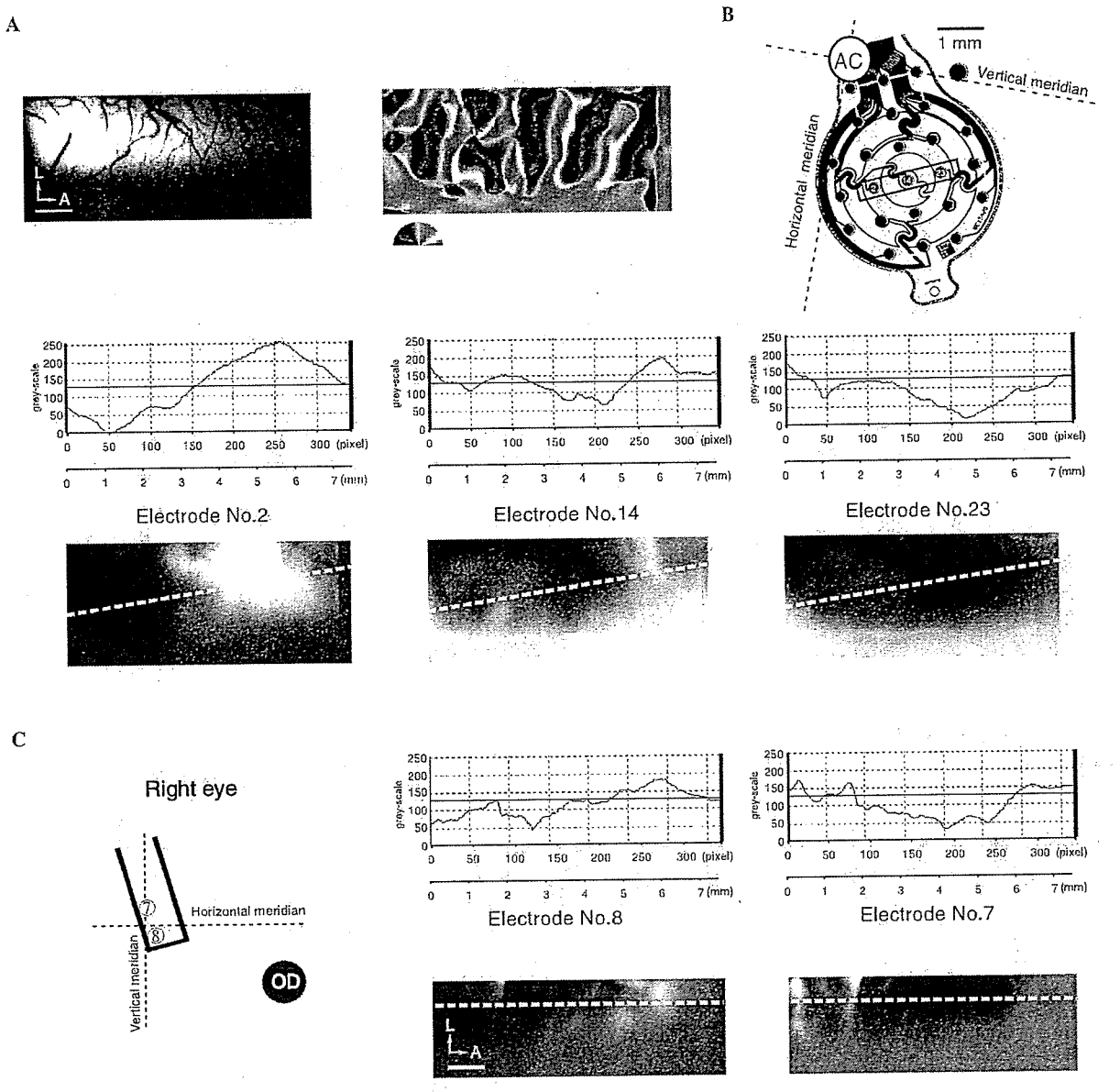

Fig. 3. Optically recorded cortical activations by visual (A), electrical epi- (B), and sub-retinal (C) stimulation with neighboring retinal electrodes. (A) Visual stimulation through a stationary horizontally oriented slit (0,5° width, 40° length) with a moving grating (see Section 2) positioned at vertical retinal eccentricities (elevation) corresponding (from left to right) to the electrode positions 2, 14, 23 in (B). The optical recordings demonstrate the spread and retinotopic displacement of visually evoked cortical activation profiles in cat area 18 (SCMs, see Section 2). (B and C) Optically recorded activation profiles (SCMs) during stimulation with spatially displaced retinal electrodes. Graphs above each optical image show one dimensional activation profiles transformed from the intensity (gray scale) levels along the broken lines (minima represent maximal activation). Considerable cortical activation is represented by the darkest black spots. They move successively from left to right with visual and electrical stimuli and are of similar size with visual and electrocal stimuli. Differences are mainly due to the long slit visual and the focal electrical stimulation. The optical images show responses to stimulation of neighboring electrodes separated by 750 μm (epi-retinal, (B); stimulation current: ±150 μA, 250 μs for each phase) and 330 μm (sub-retinal, (C); stimulation current: ±50 μA, 1 ms for each phase), and reveal activity shifts up to 3,7 mm along the anterior–posterior axis of the cortex (B). Importantly, the cortical magnification factor decreases about exponentially with increasing distance from the projection of the area centralis, and the shifts of the activated cortical locations correspond well to the published retinotopic maps (Tusa et al., 1978; Tusa et al., 1979). The exact position of the stimulation electrodes resulting in the activity images in (B and C) are shown in corresponding insets. Scale bars at optical images 1 mm in (A–C). L, lateral, A, anterior.

analyzed. Fig. 4A shows example montages in which the averaged population responses in the optic tract to single site stimulation are plotted together with the applied current amplitudes. Two important facts are demonstrated here. First, the currents for evoking similar response amplitudes differ by a factor of up to ~20 (from ±4 to ±78 μA;

Table 1
Spatial resolutions obtained with epi- and sub-retinal stimulation

Cortical recording	Epi-retinal stimulation	Sub-retinal stimulation
Optical	2.50° (thin-film electrodes)	2.50° (thin-film electrodes)
Microelectrode array	0.68° (cone electrodes)	
Microelectrode array	1.20° (thin-film electrodes)	0.90° (thin-film electrodes) 1.30° (thin-film electrodes)

The spatial resolution for microelectrode array recordings represents the resolution of the primary response. The lower resolution obtained with optical recordings corresponds well to the spatial resolution of the late responses of microelectrode recordings (see text). The high resolution of 0.68° with epi-retinal stimulation were not obtained with currently available and implantable electrode arrays but with singly in the eye inserted microelectrodes having cone-shaped tips.

epi-retinal stimulation). Second, the response delays (2–3 ms) and their durations (1–2 ms) are very short, indicating that the electrical impulses activate ganglion cells directly and evoke only a single spike per neuron (with epi- and sub-retinal stimulation, Fig. 4A). Fig. 4B shows responses to short light flashes recorded for comparison with the same optic tract electrodes. The composite visually and electrically evoked field responses were observed in a range of 30–200 μV. Compared with the responses to electrical stimuli (delay: 2–3 ms, duration: 1 ms) the visual responses have much longer latencies (~20 ms) and duration (20–35 ms) as is typical for visual population responses in the optic tract to which single ganglion cells generally contribute sequences of several spikes at a broad range of delays and with a higher degree of jitter compared to electrical impulse activation.

3.3. Activation of cortical neurons

3.3.1. Temporal precision of primary cortical action potentials

Retinal electrical stimuli evoked single impulses in ganglion cells with a repetition jitter of <1 ms (Figs. 4 and 5). Because signal transmission across geniculate synapses is highly stable in the applied frequency range of electrical stimulation (Eysel, Grüsser, & Pecci Saavedra, 1974) effective activation volleys will arrive at the primary cortical synapses also with low temporal jitter. Hence, primary cortical spikes can also be generated with high temporal precision. This is demonstrated in Fig. 5. The retino-cortical delay for the first evoked spike in this example is about 6 ms with a jitter <1 ms. For a given cortical recording location, delay and jitter depend on stimulation current and electrode type. The stronger the retinal activation the shorter the latency and the less variable the response. Fig. 5 also shows a pause after the primary spikes of about 2 ms followed by a less precise second spike. We cannot decide on our present data whether the second spikes are due to a primary activation by parvo- or konio-cellular afferents or whether they are secondary spikes in response to magnocellular input (for comparison of these cell types, see: Xu, Ichida, Allison, Bonds, & Casagrande, 2001). In summary, our results show that the visual pathway, from electrical stimulation of retinal ganglion cells to the primary responses in visual cortex, shows a high temporal precision,

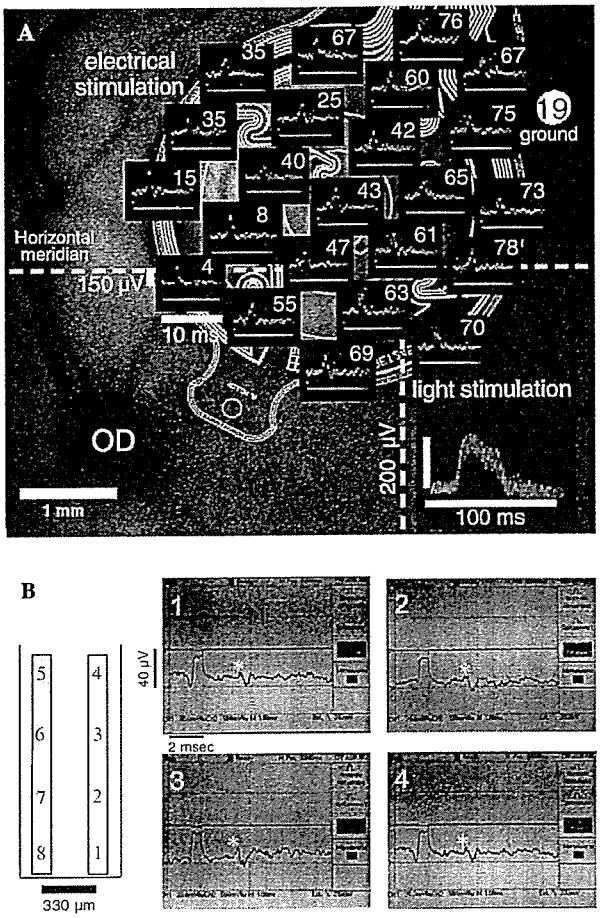

Fig. 4. Epi- and sub-retinal stimulation with thin-film electrodes and population spike recordings from the optic tract. (A) Image of the retinal implant (inter-electrode distance 750 μm) in the upper nasal quadrant of the retina overlapping area centralis. Schematic montage of thin-film array in front of retinal background superimposed by average response waveforms (small insets) evoked by short, single biphasic stimuli (±4 to ±78 μA; balanced current; waveform: 250 μs negative; 250 μs off; 250 μs positive) delivered at 1 Hz via single electrodes of the implant against ground (19). Optic tract recordings were made with a concentric bipolar tungsten electrode (SNEX-100, Rhodes Medical, Woodland Hills, CA, USA). For positioning of the recording electrode and comparison to electrical stimulation, recordings were made during 1 Hz stroboscopic light stimulation (lower right inset). Note the difference in the latency from stimulus onset to the peak responses for optical (about 20 ms) and electrical stimulation (about 2.5 ms). OD: optic disk. (B) Position of the dual in line thin-film array relative to area centralis (case S-R02) is shown to the left. The tip of the array (electrodes 1, 8) covered the foveal zone whereas the other electrodes extended along the vertical meridian in the upper hemi-retina (inter-electrode distance 330 μm). Evoked potentials to electrical stimulation (50 μA, biphasic current pulses, averaged response to 128 identical repetitions) delivered by electrodes 1, 2, 3, and 4, respectively, against the combined electrodes 5–8 of the implant as ground. Please note the slightly longer latency (about 3 ms) after sub-retinal in comparison to epi-retinal electrical stimulation.

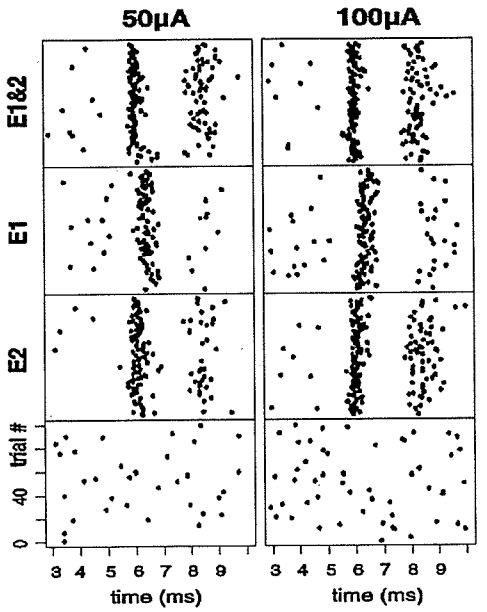

Fig. 5. Variability of cortical single unit spike responses to single site epi-retinally applied impulse-pairs (2 × 0.2 ms at 50µA (A) and 100µA (B)). The raster plots of 32 identical stimulus repetitions show from top to bottom: retinal stimulation via cone electrodes E1 and E2 synchronously, E1 and E2 separately, and maintained activity (no stimulation). Note the short retino-cortical activation delays of ~6 ms for the first spikes. Note also that the higher stimulus current (B) and the synchronous stimulation of E1 and E2 (A, B top row) lead to higher numbers of spikes and reduced temporal jitter.

because the relatively slow retinal input stages (phototransduction, synaptic transmission in the retinal network) are not in use. However, temporal resolution in visual perception should also be limited by the temporal properties of cortical circuits. These upper limits can be estimated from the time courses of cortical population responses (MUA, LFP) to electrical retinal impulse stimuli.

3.3.2. Resolution from signal approach

One coarse method for estimating the temporal resolution from the cortical responses is the measurement of the response duration at a certain amplitude (e.g., 10% of maximum). Figs. 1 and 2 (inset) show a variety of cortical peristimulus time histograms (PSTHs) in response to repetitions of single electrical impulses. In these examples, response durations are about 40–100 ms corresponding to an upper frequency limit of about 25–10 Hz. It is known that the retino-cortical pathway changes its temporal transfer properties with the rate of stimulation. This was found with stimulus patterns (Gamma interval distributions) which were systematically varied in their average impulse rates between 1 and 80 imp/s (Eger et al., 2005; Wilms et al., 2003).

Table 2 shows the average values of temporal resolutions obtained with epi- and sub-retinal stimulation. The types of electrodes, two-dimensional thin-film and three-dimensional cone-shaped stimulation electrodes revealed about the same values. Temporal resolutions with sub-retinal stimulation are only slightly lower compared to those

Table 2
Temporal resolutions for focal epi- and sub-retinal stimuli obtained from cortical microelectrode recordings, estimated directly from response time courses of microelectrode recordings (LFP)

Cortical recording	Epi-retinal stimulation	Sub-retinal stimulation
Microelectrode array	33 ms or 30/s (cone electrodes)	40 ms or 25/s (thin-film electrode)
Microelectrode array	33 ms or 30/s (thin-film electrode)	45 ms or 22/s (thin-film electrode)

The temporal resolution is derived from the duration of the activation period t/ms and is also expressed in possible frames/s (1000/activation period).

with epi-retinal stimulation. This might be due to the longer and slower retinal pathway including bipolar and ganglion cells with the sub-retinal activations while epi-retinal stimulation directly activate ganglion cells.

As the results for temporal resolutions in Table 2 were derived from averaged responses and therefore do not reveal the variability of responses to single stimuli we chose another approach. Here, we have applied information theory that can capture the amount of stimulus–response information by taking the variability of cortical responses to single impulses quantitatively into account.

3.3.3. Resolutions from information approach

The rate of information, transmitted by a stimulus train with Gamma interval distribution (Eger et al., 2005) to a single cortical recording site was calculated for identical sequences of focal light flashes and electrical impulses applied to the same retinal site. Patterns of light flashes at rates between 2 and 10 Hz show a maximum of transmitted information of about 20–40 bit/s. At high flash rates (20–50 Hz) transmission of information steeply declined, probably due to the retinal high frequency cut-off above 10 Hz (e.g., Shapley & Victor, 1981). While most of the LFP recordings showed a clear maximum, this was only the case in few MUA recordings, most likely due to the different spatial ranges contributing to an LFP and MUA recording. With stochastic stimulus sequences striking differences between electrical and visual stimulation were observed. First, in contrast to visual stimulation (with a spread of information across several recording locations) electrical stimulation delivered high rates of information only to single focal cortical patches (input range of a single cortical recording location) with very little information spread towards neighboring cortical locations. Second, using electrical stimulation and cortical LFP recordings, information rates increased continuously in parallel with stimulation rates up to the highest applied rate of 80 Hz (details in Eger et al., 2005) whereas they showed a peak at 4–8 Hz flash rates when visual stimuli were applied.

4. Discussion

The most important results are the relatively high spatial and temporal resolutions obtained with electrical retina activations in the visual cortex: about 1° visual angle (Table 1)

and 25 Hz (Table 2). Epi-and sub-retinal stimulation revealed similar results. As our resolution estimates were derived from recordings in primary visual cortex, there are good reasons to believe that they can directly be related to visual perception in the blind with retinal implants, as is argued below.

4.1. Spatial resolution

Spatial resolution was estimated on the basis of the retino-cortical spread of activation in response to a focal electrical stimulation of the retina (Table 1). We transformed this retino-cortical point spread function to degrees of visual angle in visual space at a reference eccentricity of 2° (see Section 2; assumed average electrode eccentricity of retinal implants). From the point of view of human application the cortical activation spread is an important measure because it is directly related to the spatial extent of perceived phosphenes, and cortical neurons outside the activation range, not coupled to the focal stimulus, will thus not contribute to perception. The cortical activation spread, on the other hand, may underestimate the actually obtainable spatial resolution, because stimulation with focal visual stimuli results in comparable cortical distributions of activity (Fig. 3A; see also Grinvald, Lieke, Frostig, & Hildesheim, 1994) and are associated with visual perceptions of much higher resolutions.

With the current technology of retinal stimulation, we could not activate individual ganglion cells in isolation by a single electrical impulse, instead we evoked near-synchronized responses from a spatially circumscribed population of cells in the retina. Each activated ganglion cell contributed only with a single spike to epi- and sub-retinal impulse stimuli (Figs. 4 and 5). In contrast to this, in the isolated chick retina, sub-retinal single impulse stimuli evoked groups of action potentials in retinal ganglion cells (Stett et al., 2000). The spatial resolution derived from these in vitro experiments was between 50 and 100 μm on the retina and corresponded to a retinal spatial resolution of 0.3–0.5°, as has been shown in rats suffering from complete retinal degeneration as well (RCS-rats) by the same technology.

Quite importantly, we could not differentiate which types and combination of types of retinal ganglion cells were activated, i.e., on- or off-center, magno-, parvo- or konio-cellular neurons (for cell types, see: Nirenberg, Carcieri, Jacobs, & Latham, 2001; Waessle & Boycott, 1991). We assume, however, that all types contributed to the population responses. This may render vision transmitted by such arrays as color-less since the S-, M-, and L-cone systems would be activated simultaneously. This has experimentally been confirmed with epi-retinal stimulation in human subjects evoking phosphenes that were reported as *bright*, not *dark* (Humayun et al., 1999). It also implies that we were not able to activate the retino-cortical network with electrical stimulation in the same way as with visual stimuli. Accordingly, with electrical stimulation, local contrasts will probably be processed at lower spatial and intensity resolutions than are obtained with visual stimuli in the intact system. In addition, perceptual resolutions may not adequately be estimated by the activity distributions obtained by extracellular microelectrode recordings of LFP and optical imaging signals. Both types of signals are correlated with the local superpositions of post-synaptic potentials without significant contributions from action potentials (Grinvald et al., 1994; Grinvald et al., 1999; Mitzdorf, 1987). Excitatory and inhibitory neurons contribute to these signals and it remains unclear how they are precisely related to perceptual resolution. The spatial resolutions calculated from the width of cortical activation profiles after electrical stimulation in the anesthetized cat retina should therefore be taken as a conservative approach most probably underestimating the obtainable perceptual spatial resolution in humans.

The smallest cortical activation profiles were represented by the early cortical components (10–20 ms) in response to the afferent input volley (layers 4 and 6 in area 17; Fig. 1). Previous work showed that early cortical components evoked by visual stimuli (30–50 ms post-stimulus) code local visual properties, including contour orientation, contrast and movement direction (Eckhorn, Frien, Bauer, Woelbern, & Kehr, 1993; Shevelev, Eysel, Lazareva, & Sharaev, 1998), while later components are mainly influenced by cortico-cortical interactions representing visual context (Gail, Brinksmeyer, & Eckhorn, 2000; Lamme, Rodriguez-Rodriguez, & Spekreijse, 1999). Correspondingly, later cortical responses to electrical stimulation are probably dominated by cortico-cortical lateral and feedback interactions from outside the classical RF (Angelucci et al., 2002; Bullier et al., 2001), which explains the observed dynamic expansion of the activation spread by factors of 2 to 3 during the later 50–100 ms of the response profiles (Fig. 1; see also Wilms et al., 2003). This might also partially explain the larger spread seen with the optical imaging method that is characterized by a low temporal resolution making it inevitable to include later—though also weaker—parts of the responses (Kisvarday et al., 2001).

Interestingly, two types of cortical response profiles were obtained, single- and double peak activity distributions (Fig. 2). We assume that double peaks seen with epi-retinal stimulation might be due to the simultaneous activation of local ganglion cell bodies and passing axons of slightly remote ganglion cells having offset receptive fields (Wilms & Eckhorn, 2005). In this regard, future studies using voltage sensitive dye imaging will be helpful for tracking the spatio-temporal evolution of cortical activity to single vs. multisite activation of the retinal implant.

4.1.1. Influence of electrode size on spatial resolution

The size of the thin-film stimulation electrodes considerably influence the width of the estimate of the cortical activation profile, if their diameter is larger than about 50 μm. At the cat's retinal surface, one millimeter corresponds to about 5° visual angle, i.e., 50 μm is about 0.25° (15′) (in the human eye 1 mm corresponds to approximately 3.4°;

Drasdo & Fowler, 1974). The thin-film electrodes normally used by us had contact points of 100 μm diameter. Thus, a single electrode already covered 0.5° of visual angle and accordingly the spread of retinal and cortical activation covered even larger angles of visual representation. In fact, electrodes giving rise to more localized high current densities like the fiber-cone electrodes with ~20 μm base diameter (Reitböck, 1983) revealed highest resolutions of about 0.7° with epi-retinal stimulation while epi-retinal film electrodes of 100 μm diameter reached only 1.2° (estimated from cortical response distribution; normalized to reference eccentricity of 2°, see Section 2). With sub-retinal stimulation (film electrodes, rectangular electrode areas 100 × 100 μm) similar resolutions were obtained (0.9° to 1.3°; see Table 1).

4.1.2. Influence of recorded signal type

In electrical recordings by microelectrodes, the width of the cortical activation depends on the spatial recording characteristics ("seeing" ranges) of the electrodes and the particular properties of the recorded neural signals, which are different for different signal types. The spatial spread of multiple unit activity (MUA) is in the range of 40 μm in the upper layers of area 17 of the cat (Gray, Maldonado, Wilson, & McNaughton, 1995) and of local field potentials (LFP) about 400 μm (measured with current injection and recording by a linear array of microelectrodes by the authors of the Neurophysics group, University of Marburg). Both values are cortical distances for half height decline. For the smallest measured width of cortical activations (around 1 mm here) this means that we potentially overestimated values based on MUA by about 8% and those with LFP by 80%. However, these influences must be considered in conjunction with the effective lateral coupling width of the neural network involved in the stimulus evoked responses and with the size and form of the stimulation electrodes.

The recording technique of optical imaging captures averaged signals from the cortical surface down to a depth of approximately 700 μm. The recorded intrinsic signals are mainly based on the oxygen consumption and the related deoxygenation of hemoglobin in active cortical regions (for review, see Grinvald et al., 1999); their spatial resolution is influenced by the intercapillary distances in the brain (approximately 50 μm in the cat visual cortex). Inhibitory and excitatory post-synaptic potentials as well as spike responses contribute to the intrinsic signals. Thus, they represent above threshold spike responses and all subthreshold synaptic activity, which all contribute to the width of the distribution of intrinsic signal changes evoked by retinal stimulation.

4.1.3. Influence of lateral connectivities

Our estimate of the spatial resolution on the basis of the cortical activation width may also depend on the effective lateral couplings among evoked signals in the retina, geniculate nucleus, and cortex, which are due to the lateral connectivities in these structures. They include divergent excitatory feed forward connections, of which magno cellular geniculate neurons are particularly broadly projecting to the cortex (Freund, Martin, Soltesz, Somogyi, & Whiteridge, 1989; Humphrey, Saul, & Feidler, 1998) and lateral intracortical facilitatory and disinhibitory connections (Kisvarday & Eysel, 1992). The superimposed influences of all these connectivity-based lateral spreads of activation are about 2–3 mm in the cat primary visual cortex (half height decline measured by signal correlations; Brosch, Bauer, & Eckhorn, 1991). Hence, these widths are equal or even larger than the highest resolutions given in our present report. This is due to the fact that we could take the early cortical response components (from the electrical recordings) which are locally confined, whereas the lateral spread of the activation increases considerably about 20 ms after stimulation (Fig. 1A).

The estimated minimal requirements of spatial resolution for useful artificial vision, investigated by psychophysical methods can be compared and combined with our physiological estimates of achievable spatial resolution under optimal conditions. Reading at central retinal projection sites requires about 300 pixels (20 × 15) within about 5° retinal eccentricity (Sommerhalder et al., 2003). If we take a physiologically achievable resolution of 0.75° and substitute each image pixel by a stimulation electrode with constant spacing, the stimulation array will cover 3.9 by 2.8 mm^2 retina (~7.1° by ~5.3° visual eccentricity). If safe navigation in dynamic out-door environments is required, stimulation should include eccentricities of at least 15° (Cha, Horch, Normann, & Boman, 1992b; Geruschat et al., 1998). Since the spatial resolution required for safe navigational purposes outside the reading area can be chosen much coarser (at about 2° electrode pitch) this would add about another 200 electrodes for the outer "navigational belt." Hence, as a minimal condition a total of about 500 well functioning electrodes with comparable stimulation capabilities would be required for an implant usefully spanning a retinal stimulation area of about 8 mm in diameter.

4.2. Temporal resolution

The rate of possible temporal modulation can coarsely be estimated from the duration of cortical responses to single electrical impulses applied in the retina. With stimulus currents twice the threshold we measured response durations of about 40 ms at one second stimulus repetitions. However, with higher stimulation rates of 10–50 impulses per second mimicking more natural interval distributions (Gamma), response durations decreased considerably (to 20–30 ms, estimated from the stimulus–response cross-correlations). This corresponds to an increase in temporal resolution which can be caused by several factors such as an increase in the average level of cortical inhibition that keeps the late response phases subthreshold. In addition, higher stimulation rates lead to increased average activations of both excitatory and inhibitory synapses which, in turn, reduce the time constants and increase the frequency

bandwidths of dendrites and somata of ortical neurons (Agmon-Snir & Segev, 1993; Nelson, 1994). Hence, near physiological patterns and high rates of retinal stimulation can result in cortical response durations which are able to code 30–50 temporal changes of two-level intensities per second. However, the pilot experiments of Humayun et al. (1999) with electrical stimulation in human patients suggest somewhat lower frequencies. They created non-flickering perception with rhythmic stimulation already at frequencies between 40 and 50 Hz. Nonetheless, fast temporal changes may be also perceiveable with non-rhythmic (stochastic) stimulation patterns generating non-rhythmic spike patterns in ganglion cells similar to visual responses.

4.2.1. Discrimination among somal and axonal stimulations

We found that epi-retinal stimulation has to deal with the problem of activation of ganglion cell somata in the vicinity of the electrode tip and of passing axons originating from remote ganglion cell bodies (results not shown here). This problem cannot be neglected, since a simultaneous activation of ganglion cell bodies in the vicinity of the electrode and passing axons may lead to multisite or ambiguous phosphenes (Wilms & Eckhorn, 2005). For a solution of this problem further investigations are required. Cone electrodes protruding to ganglion cell somata through the internal limitating membrane could selectively activate the cell bodies. For selective fiber stimulation, electrode pairs with tips aligned parallel to the fibers and specific stimulation current/time patterns might provide a solution. Finally, offsets of single focal phosphenes due to activation of passing fibers by epi-retinal electrodes can be compensated by an adaptable retina-processor outside of the eye (Eckmiller, 1997). On the other hand, sub-retinal stimulation at retinal eccentricities smaller than 8° would have to face systematic and increasing mislocation of phosphenes with decreasing eccentricity due to the displacement of bipolar and retinal ganglion cells in the central retinal region (Sjöstrand, Olsson, Popovic, & Conradi, 1999). However, the physiological resolution providing a visual acuity of 0.1–0.2 at the desired location of 8° eccentricity corresponds well with the spatial characteristics of sub-retinal chips.

5. Conclusions

We obtained relatively high spatial and temporal resolutions of 0.7–1.3° visual angle and 30–40 ms, respectively, with both epi- and sub-retinal stimulation. Spatial resolution can

Fig. 6. Real scenes filtered with resolutions obtained in this investigation. (A) Person at the end of a tunnel; (B) person standing in a hall; (C) group of persons on a street. (a) Unfiltered; (b) resampled on a regular cartesian raster; (c) resampled on a irregular hexagonal grid with spatial frequency increasing from periphery to center. Highest resolution is centered on the person at the end of the tunnel (A), head of person (B and C). Gaussian filter kernels at 500 grid positions, simulating Gaussian shaped phosphenes evoked by 500 stimulation electrodes. The output images are restricted to 8 gray tones.

probably be increased up to 0.5° visual angle by choosing smaller-area flat or cone tip electrodes made from materials with higher charge transfer capacity. The highest resolution estimates were reported for electrical stimulation in isolated retinae (Stett et al., 2000) which may be 0.3° visual angle. The upper limit obtained for temporal resolution can further be increased by using higher stimulation rates, mimicking physiological spike patterns of retinal ganglion cells. Since the resolutions reported here were estimated from cortical recordings, direct relations to visual perception are possible, including the expected perception by the blind patients, but may underestimate the finally achievable resolution. We assume that the resolutions obtainable with electronic retinal implants are sufficient for visuo-motor coordination in many in- and out-door situations of daily life. We demonstrate this by movie presentations of simulated perceptions (example clips in Fig. 6) obtained by filtering typical visual scenes with the resolution values obtained in this investigation (accessible under http://neuro.physik.uni-marburg.de/~retina-implant/). Our results indicate that spatial resolution achieved by sub- or epi-retinal stimulation should be sufficient to gain useful object recognition in dynamic environments.

Acknowledgments

The authors acknowledge the cooperation of many colleagues involved in the project (for the presentation of the consortium, see www.uni-tuebingen.de/rim and www.nero.uni-bonn.de and www.neuro.physik.uni-marburg.de/~retina-implant). We also are very grateful for the support by the German Ministry of Research and Technology (01KP0007, 01KP0008) and for the Support by Pro Retina Deutschland e.V. and the Ewald und Karin Hochbaum-Foundation.

References

Adams, D. L., & Horton, J. C. (2003). A precise retinotopic map of primate striate cortex generated from the representation of angioscotomas. *Journal of Neuroscience, 23*, 3771–3789.

Agmon-Snir, H., & Segev, I. (1993). Signal delay and input synchronization in passive dendritic structures. *Journal of Neurophysiology, 70*, 2066–2085.

Angelucci, A., Levitt, J. B., Walton, E. J. S., Hupé, J.-M., & Bullier, J. (2002). Circuits for local and global signal integration in primary visual cortex. *Journal of Neuroscience, 22*, 8633–8646.

Bonhoeffer, T., & Grinvald, A. (1996). Optical imaging based on intrinsic signals. The methodology. In A. W. Toga & J. C. Mazziotta (Eds.), *Brain mapping: The methods* (pp. 55–97). San Diego: Academic Press.

Brosch, M., Bauer, R., Eckhorn, R. (1991). Spatial correlation profiles of stimulus-induced oscillatory activities in cat visual cortex. *Proceedings of the Goettingen Neurobiology Conference*, New York: Thieme, p 214.

Bullier, J., Hupe, J.-M., James, A. C., & Girard, P. (2001). The role of feedback connections in shaping the responses of visual cortical neurons. *Progress in Brain Research, 134*, 193–204.

Cha, K., Horch, K. W., & Normann, R. A. (1992a). Mobility performance with a pixelized vision system. *Vision Research, 32*, 1367–1372.

Cha, K., Horch, K. W., Normann, R. A., & Boman, D. (1992b). Reading speed with a pixelized vision system. *Journal of the Optical Society of America A, 9*, 673–677.

Chow, A. Y., & Chow, V. Y. (1997). Subretinal electrical stimulation of the rabbit retina. *Neuroscience Letters, 225*, 13–16.

Chow, A. Y., Pardue, M. T., Chow, V. Y., Peyman, G. A., Liang, C., Perlman, J. I., et al. (2001). Implantation of silicon chip microphotodiode arrays into the cat subretinal space. *IEEE Transactions on Neural Systems and Rehabilitation Engineering, 9*, 86–95.

Chow, A. Y., Pardue, M. T., Perlman, J. I., Ball, S. L., Chow, V. Y., Hetling, J. R., et al. (2002). Subretinal implantation of semiconductor-based photodiodes: Durability of novel implant designs. *Journal of Rehabilitation Research and Development, 39*, 313–321.

Darian-Smith, C., & Gilbert, C. D. (1995). Topographic reorganization in the striate cortex of the adult cat and monkey is cortically mediated. *Journal of Neuroscience, 15*, 1631–1647.

Dinse, H., & Krüger, K. (1994). The timing of processing along the visual pathway in the cat. *Neuroreport, 5*, 893–897.

Drasdo, N., & Fowler, C. W. (1974). Non-linear projection of the retinal image in a wide angle schematic eye. *British Journal of Ophthalmology, 58*, 709–714.

Eckhorn, R., & Pöpel, B. (1975). Rigorous and extended application of information theory to the afferent visual system of the cat. II. Experimental results. *Biological Cybernetics, 17*, 7–17.

Eckhorn, R., Grüsser, O.-J., Kröller, J., Pellnitz, K., & Pöpel, B. (1976). Efficiency of different neural codes: Information transfer calculations for three different neuronal systems. *Biological Cybernetics, 32*, 243–248.

Eckhorn, R., & Pöpel, B. (1981). Responses of cat retinal ganglion cells to the random motion of a spot stimulus. *Vision Research, 21*, 435–443.

Eckhorn, R., Frien, A., Bauer, R., Woelbern, T., & Kehr, H. (1993). High frequency (60–90 Hz) oscillations in primary visual cortex of awake monkey. *Neuroreport, 4*, 243–246.

Eckhorn, R., & Thomas, U. (1993). A new method for the insertion of multiple microprobes into neural and muscular tissue, including fiber electrodes, fine wires, needles and microsensors. *Journal of Neuroscience Methods, 49*, 175–179.

Eckmiller, R. (1997). Learning retina implants with epiretinal contacts. *Ophthalmic Research, 29*, 281–289.

Eger, M., Wilms, M., Eckhorn, R., & Schanze, T. (2005). Information transmission from a retina implant to the cat visual cortex. *Biosystems, 79*, 133–142.

Eysel, U. T., Grüsser, O.-J., & Pecci Saavedra, J. (1974). Signal transmission through degenerating synapses in the lateral geniculate body of the cat. *Brain Research, 76*, 49–70.

Freund, T. F., Martin, K. A. C., Soltesz, I., Somogyi, P., & Whiteridge, D. (1989). Arborisation pattern and postsynaptic targets of physiologically identified thalamocortical afferents in striate cortex of the macaque monkey. *Journal of Comparative Neurology, 289*, 315–336.

Gail, A., Brinksmeyer, H. J., & Eckhorn, R. (2000). Contour decouples gamma activity across texture representation in monkey striate cortex. *Cerebral Cortex, 10*, 840–850.

Gekeler, F., Kobuch, K., Schwahn, H. N., Stett, A., Shinoda, K., & Zrenner, E. (2004). Subretinal electrical stimulation of the rabbit retina with acutely implanted electrode arrays. *Graefes Archiv of Clinical and Experimental Ophthalmology, 242*, 587–596.

Geruschat, D. R., Turano, K. A., & Stahl, J. W. (1998). Traditional measures of mobility performance and retinitis pigmentosa. *Optometry and Visual Sciences, 75*, 525–537.

Gilbert, C. D., & Wiesel, T. N. (1990). The influence of contextual stimuli on the orientation selectivity of cells in primary visual cortex of the cat. *Vision Research, 30*, 1689–1701.

Gilbert, C. D. (1993). Circuitry, architecture, and functional dynamics of visual cortex. *Cerebral Cortex, 3*, 373–386.

Gray, C. M., Maldonado, P. E., Wilson, M., & McNaughton, B. (1995). Tetrodes markedly improve the reliability and yield of multiple single-unit isolation from multi-unit recordings in cat striate cortex. *Journal of Neuroscience Methods, 63*, 43–54.

Grind van de, W. A., Grüsser, O. J., & Lunkenheimer, H. U. (1973). Perception and physiology of flicker vision. In *Central processing of visual information. A: Integrative functions and comparative data, handbook of sensory physiology* (Vol. VII/3). Berlin, New York: Springer.

Grinvald, A., Lieke, E., Frostig, R., & Hildesheim, R. (1994). Cortical point spread function and long-range lateral interactions revealed by real-time optical imaging of macaque monkey primary visual cortex. *Journal of Neuroscience, 14*, 2545–2568.

Grinvald, A. D., Shoham, A., Shmuel, D. E., Glaser, I., Vanzetta, E., Shtoyerman, H., et al. (1999). In-vivo optical imaging of cortical architecture and dynamics. A. In U. Windhorst & H. Johansson (Eds.), Modern techniques in neuroscience research. Springer, pp. 893–969.

Grüsser, O.-J., & Creutzfeld, O. (1957). Eine neurophysiologische Grundlage des Brücke-Bartley-Effektes: Maxima der Impulsfrequenz retinaler und corticaler Neurone bei Flimmer-Licht mittlerer Frequenzen. *Pflügers Archiv der gesamten Physiologie, 263*, 668–681.

Hesse, L., Schanze, T., Wilms, M., & Eger, M. (2000). Implantation of retina stimulation electrodes and recording of electrical stimulation responses in the visual cortex of the cat. *Graefe's Archiv of Clinical and Experimental Ophthalmology, 238*, 840–845.

Heydt von der, R., & Peterhans, E. (1989). Mechanisms of contour perception in monkey visual cortex. I. Lines of pattern discontinuity. *Journal of Neuroscience, 9*, 1731–1748.

Hubel, D., & Wiesel, T. (1962). Receptive fields, binocular interaction, and functional architecture in the cat's visual cortex. *Journal of Physiology, 160*, 106–154.

Humayun, M. S., Probst, R. H., Juan, E. de., McCormick, K., & Hickingbotham, D. (1994). Bipolar surface electrical stimulation of the vertebrate retina. *Archive of Ophthalmology, 112*, 110–116.

Humayun, M. S., Juan, E. de., Dagnelie, G., Greenberg, R. J., Probst, R. H., & Phillips, D. H. (1996). Visual perception elicited by electrical stimulation of retina in blind humans. *Archive of Ophthalmology, 114*, 40–46.

Humayun, M. S., Juan, E. de., Weiland, J. D., Dagnelie, G., Katona, S., Greenberg, R., et al. (1999). Pattern electrical stimulation of the human retina. *Vision Research, 39*, 2569–2576.

Humayun, M. S., Weiland, J. D., Fujii, G. Y., Greenberg, R., Williamson, R., Little, J., et al. (2003). Visual perception in a blind subject with a chronic microelectrode retinal prosthesis. *Vision Research, 43*, 2573–2581.

Humphrey, A. L., Saul, A. B., & Feidler, J. C. (1998). Strobe rearing prevents the convergence of inputs with different timings onto area 17 simple cells. *Journal of Neurophysiology, 80*, 3005–3020.

Kisvarday, Z. F., Buzas, P., & Eysel, U. T. (2001). Calculating direction maps from intrinsic signals revealed by optical imaging. *Cerebral Cortex, 11*, 636–647.

Kisvarday, Z. F., & Eysel, U. T. (1992). Cellular organization of reciprocal patchy networks in layer III of cat visual cortex (area 17). *Neuroscience, 46*, 275–286.

Knierim, J. J., & van Essen, D. C. (1992). Neuronal responses to static texture patterns in area V1 of the alert macaque monkey. *Journal of Neurophysiology, 67*, 961–980.

Lamme, V. A. F., Rodriguez-Rodriguez, V., & Spekreijse, H. (1999). Separate processing dynamics for texture elements, boundaries and surfaces in primary visual cortex of the macaque monkey. *Cerebral Cortex, 9*, 406–413.

Legge, G. E., Ahn, S. J., Klitz, T. S., & Luebker, A. (1997). The visual span in normal and low vision. *Vision Research, 37*, 1999–2010.

Mitzdorf, U. (1987). Properties of the evoked potential generators: Current source-density analysis of visually evoked potentials in cat cortex. *The Journal of Neuroscience, 33*, 33–59.

Nelson, M. E. (1994). A mechanism for neuronal gain control by descending pathways. *Neural Computation, 6*, 242–254.

Nirenberg, S., Carcieri, S. M., Jacobs, A. L., & Latham, P. E. (2001). Retinal ganglion cells act largely as independent encoders. *Nature, 411*, 698–701.

Normann, R. A., Maynard, E. M., Guillory, K., & Warren, D. J. (1996). Cortical implants for the blind. *IEEE Spectrum, 33*, 54–59.

Normann, R. A., Maynard, E. M., Rousche, P. J., & Warren, D. J. (1999). A neural interface for a cortical vision prosthesis. *Vision Research, 39*, 2577–2587.

Orban, G. A. (1984). *Neuronal operations in the visual cortex*. Berlin, New York: Springer.

Peyman, G., Chow, A. Y., Liang, C., Chow, V. C., Perlman, J. I., & Peachey, N. S. (1998). Subretinal semiconductor microelectrode array. *Ophthalmic Surgery and Lasers, 29*, 234–241.

Rager, G., & Singer, W. (1998). The response of cat visual cortex to flicker stimuli of variable frequency. *European Journal of Neuroscience, 10*, 1856–1877.

Ratzlaff, E. H., & Grinvald, A. (1991). A tandem-lens epifluorescence macroscope: Hundred-fold brightness advantage for wide-field imaging. *Neuroscience Methods, 36*, 127–137.

Reitböck, H. J. (1983). Fiber microelectrodes for electrophysiological recordings. *Journal of Neuroscience Methods, 8*, 249–262.

Rieke, F., Warland, D. K., de Ruyter van Steveninck, R. R., & Bialek, W. (1998). *Spikes: Exploring the neural code*. Cambridge: MIT Press.

Rizzo, J. F., Loewenstein, J., Kelly, S., Shire, D., Herndon, T., & Wyatt, J. L. (1999). Electrical stimulation of human retina with a microfabricated electrode array. *Investigative Ophthalmology and Visual Science, 40*, S783.

Rizzo, J. F., & Wyatt, J. L. (1997). Prospects for a visual prosthesis. *The Neuroscientist, 3*, 251.

Sachs, H. G., Kobuch, K., Miliczek, K. D., Kohler, K., Zrenner, E., & Gabel, V.-P. (1999). The Yucatan micropig model for implantation of subretinal microphotodiode arrays (MPDA) in visual prosthetic research. *Investigative Ophthalmology and Visual Sciences, 40*, S734.

Salzman, C. D., Britten, K. H., & Newsome, W. T. (1990). Cortical microstimulation influences perceptual judgements of motion direction. *Nature, 346*, 174–177.

Santos, A., Humayun, M., de Juan, E., Greenburg, R. J., Marsh, M., Klock, I., et al. (1997). Preservation of the inner retina in retinitis pigmentosa. *Archive of Ophthalmology, 115*, 511–515.

Schanze, T., Wilms, M., Eger, M., Hesse, L., & Eckhorn, R. (2002). Activation zones in cat visual cortex evoked by electrical retina stimulation. *Graefe's Archiv of Clinical and Experimental Ophthalmology, 240*, 947–954.

Schwahn, H. N., Gekeler, F., Kohler, K., Kobuch, K., Sachs, H. G., Schulmeyer, F., et al. (2001). Studies on the feasibility of a subretinal visual prosthesis: Data from Yucatan micropig and rabbit. *Graefes Archive of Clinical and Experimental Ophthalmology, 239*, 961–967.

Seiler, M. J., Aramant, R. B., & Ball, S. L. (1999). Photoreceptor function of retinal transplants implicated by light–dark shift of s-antigen and rod transducin. *Vision Research, 39*, 2589–2596.

Shannon, C. E. (1948). A mathematical theory of communication. *Bell Systems Technical Journal, 27*, 623–656.

Shapley, R. M., & Victor, J. D. (1981). How the contrast gain control modifies the frequency responses of cat retinal ganglion cells. *Journal of Physiology, 318*, 161–179.

Shevelev, I. A., Eysel, U. T., Lazareva, N. A., & Sharaev, G. A. (1998). The contribution of intracortical inhibition to dynamics of orientation tuning in cat striate cortex neurons. *Neuroscience, 84*, 11–23.

Sjöstrand, J., Olsson, V., Popovic, Z., & Conradi, N. (1999). Quantitative estimations of foveal and extra-foveal retinal circuitry in humans. *Vision Research, 39*, 2987–2998.

Sommerhalder, J., Oueghlani, E., Bagnoud, M., Leonards, U., Safran, A., & Pellizone, M. (2003). Simulation of artificial vision: I. Eccentric reading of isolated words, and perceptual learning. *Vision Research, 43*, 269–283.

Stett, A., Barth, W., Weiss, S., Haemmerle, H., & Zrenner, E. (2000). Electrical multisite stimulation of the isolated chicken retina. *Vision Research, 40*, 1785–1795.

Stieglitz, T., Beutel, H., Schuettler, M., & Meyer, J. (2000). Micromachined polyimide-based devices for flexible neural interfaces. *Biomedical Microdevices, 2*, 283–294.

Sutter, E. E. (2001). Imaging visual function with the multifocal m-sequence technique. *Vision Research, 41*, 1241–1255.

Tovee, M. J. (1996). *An introduction to the visual system*. Cambridge University Press.

Tusa, R. J., Palmer, L. A., & Rosenquist, A. C. (1978). The retinotopic organization of area 17 (striate cortex) in the cat. *Journal of Comparative Neurology, 177*, 213–236.

Tusa, R. J., Rosenquist, A. C., & Palmer, L. A. (1979). Retinotopic organization of areas 18 and 19 in the cat. *Journal of Comparative Neurology, 185*, 657–678.

Volker, M., Shinoda, K., Sachs, H., Gmeiner, H., Schwarz, T., Kohler, K., et al. (2006). In vivo assessment of subretinally implanted microphotodiode arrays in cats by optical coherence tomography and fluorescein angiography. *Graefes Archiv of Clinical and Experimental Ophthalmology*, (in press).

Wachtler, T., Sejnowski, T. J., & Albright, T. D. (2003). Representation of color stimuli in awake macaque primary visual cortex. *Neuron, 37*, 681–691.

Waessle, H., & Boycott, B. B. (1991). Functional architecture of the mammalian retina. *Physiological Reviews, 71*, 447–480.

Wilms, M., Eger, M., Schanze, T., & Eckhorn, R. (2003). Visual resolution with epi-retinal electrical stimulation estimated from activation profiles in cat visual cortex. *Visual Neuroscience, 20*, 543–555.

Wilms, M., & Eckhorn, R. (2005). Spatiotemporal receptive field properties of epiretinally recorded spikes and local electroretinograms in cats. *BMC Neuroscience, 6*, 50.

Wyatt, J., & Rizzo, J. (1996). Ocular implants for the blind. *IEEE Spectrum, 33*, 47–53.

Xu, X.-M., Ichida, J., Allison, J. D., Bonds, A. B., & Casagrande, V. A. (2001). A comparison of koniocellular, magnocellular and parvocellular receptive field properties in the lateral geniculate nucleus of thed owl monkey (aotus trivirgatus). *Journal of Physiology (Lond.), 531*, 203–218.

Zrenner, E., Miliczek, K. D., Gabel, V., Graf, H., Guenther, E., Haemmerle, H., et al. (1997). The development of subretinal microphotodiodes for replacement of degenerated photoreceptors. *Ophthalmic Research, 29*, 269–280.

Zrenner, E., Stett, A., Weiss, S., Aramant, R. B., Guenther, E., Kohler, K., et al. (1999). Can subretinal microphotidiodes successfully replace degenerated photoreceptors? *Vision Research, 39*, 2555–2567.

Zrenner, E. (2002). Will retinal implants restore vision? *Science, 295*, 1022–1025.

Available online at www.sciencedirect.com
SCIENCE DIRECT®
Experimental Eye Research 83 (2006) 329–338
EXPERIMENTAL EYE RESEARCH
www.elsevier.com/locate/yexer

Expression of endostatin in human choroidal neovascular membranes secondary to age-related macular degeneration

Olcay Tatar [a], Kei Shinoda [b], Annemarie Adam [c], Jens Martin Rohrbach [a], Klaus Lucke [d], Sigrid Henke-Fahle [a], Karl Ulrich Bartz-Schmidt [a], Salvatore Grisanti [a,*]

[a] *University Eye Clinic at the Centre for Ophthalmology of the Eberhard-Karls-University Tübingen, Schleichstrasse 12-15, 72076 Tuebingen, Germany*
[b] *Laboratory of Visual Physiology, National Institute of Sensory Organs, National Hospital Organization, Tokyo Medical Center, Japan*
[c] *Department of Pathology, Eberhard-Karls-University, Tuebingen, Germany*
[d] *Eye Clinic Universitätsallee, Bremen, Germany*

Received 7 June 2005; accepted in revised form 21 December 2005
Available online 11 April 2006

Abstract

Endostatin is an endogenous angiogenesis inhibitor which requires E-selectin for its antiangiogenic activity. The aim of this study was to investigate the expression of endostatin in human choroidal neovascular membranes (CNV) secondary to age-related macular degeneration (AMD) with regard to vascularization and proliferative activity. An interventional case series of 36 patients who underwent removal of CNV were retrospectively investigated. Thirty-six CNV were analyzed by light microscopic immunohistochemistry for the expression of CD34 (endothelial cells, EC), CD105 (activated EC), Ki-67 (cell proliferation), Cytokeratin 18 (epithelial cells), VEGF (vascular endothelial growth factor), E-selectin and endostatin. Donor eyes ($n = 7$) including one with AMD were used as controls. Endostatin immunoreactivity was present in choroidal vessels of five as well as in the retinal pigment epithelium (RPE)-Bruch's membrane complex of two donor eyes without AMD. In one eye with AMD, endostatin was detected in RPE, Bruch's membrane and choroidal vessels. Ninety-two percent (33/36) of CNV disclosed endostatin staining. RPE-Bruch's membrane complex, choroidal vessels and stroma were positive in 50% (18/36), 72% (26/36), and 78% (28/36) of the membranes, respectively. Both control eyes and CNV expressed all the investigated markers except E-selectin being positive only in membranes. Endostatin, an endogenous angiogenesis inhibitor, is expressed in CNV and its therapeutic up-regulation may be a new strategy in the treatment of neovascular AMD.

Keywords: age-related macular degeneration; choroidal neovascularization; angiogenesis; endostatin; E-selectin

1. Introduction

Choroidal neovascularization (CNV) is responsible for the majority of severe visual loss due to age-related macular degeneration (AMD), the most common cause of visual morbidity in elderly (The Macular Photocoagulation Study Group, 1991). Recent studies have clarified the importance of a balance between local inhibitory and stimulatory factors in the pathogenesis of angiogenesis (Pepper, 2001), but some of these factors still remain to be defined.

Endostatin, a 20 kDa C-terminal fragment of collagen XVIII, has been identified as an endogenous angiogenesis inhibitor (O'Reilly et al., 1997). Collagen XVIII is the core protein of a heparan sulfate proteoglycan in vascular and epithelial basement membranes (Zatterstrom et al., 2000). Endostatin is bound to collagen XVIII by a protease-sensitive hinge. Some proteases, such as matrix metalloproteases (MMPs), can cleave the hinge so that endostatin can be released and becomes available (Sasaki et al., 1998; Ferreras et al., 2000).

* Corresponding author. Tel.: +49 7071 2984004; fax: +49 7071 295215.
E-mail address: salvatore.grisanti@med.uni-tuebingen.de (S. Grisanti).

0014-4835/$ - see front matter © 2006 Elsevier Ltd. All rights reserved.
doi:10.1016/j.exer.2005.12.017

The antiangiogenic effect of endostatin is both at the transcriptional and cellular level. At the transcriptional level, endostatin down-regulates proangiogenic genes related to vascular endothelial growth factor (VEGF) signalling (e.g. thrombin receptors, Stats, and HIF-1), but up-regulates antiangiogenic genes (such as Vasostatin, Kininogen) in human microvascular endothelial cells (EC) (Abdollahi et al., 2004). On the cellular level, endostatin was shown to inhibit EC proliferation and migration stimulated by FGF-2 (Eriksson et al., 2003), EC chemotactic migration towards VEGF (Eriksson et al., 2003; Yamaguchi et al., 1999) and EC invasion by blocking the activation and catalytic activity of MMP-2 (Lee et al., 2002; Kim et al., 2000). Additionally, endostatin induces EC apoptosis (Dhanabal et al., 1999; Dixelius et al., 2000). Lately, E-selectin, a cellular adhesion molecule, was proven to be required for the antiangiogenic activity of endostatin (Yu et al., 2004).

EC in different parts of the body have different characteristics (Lanzer and Raff, 1987). Variations in surrounding cells and extracellular matrix may also contribute to the tissue-specific aspects of neovascularization (Mori et al., 2001). The altered local balance between stimulators and inhibitors is accepted to be the cause of neovascularization (Pepper, 2001; Mori et al., 2001); however, the involved players may vary depending on the setting.

All the aforementioned angiogenic factors (FGF, VEGF, MMP, HIF-1) seem to have well-defined roles in the pathogenesis and development of CNV (Amin et al., 1994; Kvanta et al., 1996; Martin et al., 2004; Lambert et al., 2003). Endostatin, shown to inhibit their activities and known to up-regulate antiangiogenesis genes, therefore, is likely to be an endogenous inhibitor of angiogenesis also in CNV. Intravitreal or intravenous delivery of endostatin by viral vectors was shown to inhibit diabetic retinopathy and choroidal neovascularization in experimental studies (Mori et al., 2001; Auricchio et al., 2002). Bhutto et al. (2004) evaluated endostatin expression in five donor eyes with advanced AMD—four eyes with disciform scar with small CNV and one eye with geographic atrophy with sub-RPE neovascularization—and reported nearly absent endostatin expression. However, to the best of our knowledge, expression of this endogenous angiogenesis inhibitor in active CNV membranes extracted surgically before they reach the disciform scar stage has not been defined experimentally or clinically yet.

The aim of this study was to analyze the endostatin expression in surgically extracted active human CNV with regard to vascularization and proliferative activity. The level of vascularization was determined by the expression of CD 34, a pan-endothelial cell marker, and CD105 (Endoglin), a marker for activated endothelial cells (Grisanti et al., 2004).

Ki-67, Cytokeratin18 (CK18) and an antibody specific for VEGF-A were used to detect the proliferative activity (Grisanti et al., 2004), to identify RPE cells (Martin et al., 2004) and to evaluate the angiogenic stimulation, respectively. Expression of E-selectin which is required for the antiangiogenic activity of endostatin (Yu et al., 2004) was analyzed both in control eyes and CNV.

2. Materials and methods

2.1. Subjects and treatment

We retrospectively reviewed 36 CNV, secondary to neovascular AMD, from 36 eyes of 36 consecutive patients, in which three-port vitrectomy and extraction of CNV was performed. None of the patients had disciform scar but CNV with submacular leakage or hemorrhage leading to progressive visual deterioration. CNV membranes previously treated with photodynamic therapy, laser coagulation or any kind of anti-angiogenesis therapy including intravitreal triamcinolone injection were not included in our series. Each patient gave written informed consent after the nature of the procedure and alternatives had been fully explained. The study followed the guidelines of the declaration of Helsinki as revised in Tokyo and Venice and adhered to the requirements of the local Institutional Review Board. The histological analysis of the specimens was approved by the Institutional Ethic Committee. Normal donor eyes ($n = 6$) and a donor eye with drusen but without neovascularization ($n = 1$) received for keratoplasty were used as controls.

2.2. Tissue preparation

Within minutes after surgery, excised CNV and donor eyes were fixed in 3.7% formalin and subsequently embedded in paraffin. Each specimen was serially sectioned into 5-μm sections and mounted on poly-L-lysine coated glass slides (Dako, Glostrup, Denmark) for immunohistochemical staining. Hematoxylin–eosin and PAS staining were performed to determine the histologic orientation. PAS staining was primarily used to confirm the location of the diffuse drusen and to help the overall orientation of the specimens.

2.3. Immunohistology

After serial paraffin sections were de-paraffinized and rehydrated with a graded series of alcohol, different techniques for antigen retrieval were applied. For CK18 and endostatin, antigen retrieval was accomplished by proteolytic digestion with 0.5% protease type XXIV (Bacterial, Sigma, St. Louis, MO) whereas proteinase K (Dako) was used for VEGF. For Ki-67, CD34, CD105 and E-selectin staining, antigen retrieval was accomplished with heat treatment in citrate buffer in a pressure cooker for 2 min.

Immunohistochemical staining for CD105, CD34, Ki-67, CK18 and E-selectin was performed using the horseradish peroxidase method according to the manufacturer's protocol (Vectastain Universal Elite ABC PK-6200 kit, Vector Laboratories, Burlinghame, CA). To block endogenous peroxidase activities, 3% hydrogen peroxide and 0.1% sodium acid were applied to each section. Subsequently, the sections were incubated with horse serum (30 min). Thereafter, specimens were incubated with the primary antibodies specific for human CD105 (mouse, Mab, Clone SN6h, Dako), CD34 (mouse, Mab, Immunotech, Hamburg, Germany), Ki-67

(mouse, Mab, Clone Ki-S5, Dako), and CK 18 (mouse, Mab, Progen, Heidelberg, Germany) and E-selectin (mouse, Mab, Novocastra, UK) for 1 h at room temperature. After incubating with the biotinylated horse anti-mouse anti-rabbit secondary antibody and the ABC Complex (Vectastain Universal Elite ABC PK-6200 kit, Vector Laboratories) for 15 min, followed by washing in-between and afterwards, the antibody-treated sections were developed with a 3-diaminobenzidine (Fluka, Buchs, Germany) solution combined with H_2O_2 for CD34, CD105 and Ki-67 staining. For CK 18 and E-selectin staining, the chromogen was replaced with AEC high sensitive substrate chromogen (Cytomation, Code K3461, Dako).

Immunohistochemical stainings for VEGF and endostatin were performed by the alkaline-phosphatase method according to the manufacturer's instructions (ChemMate Detection Kit, Alkaline Phosphatase/RED, Rabbit/Mouse, K5005; Dako). Briefly, after proteolytic digestion with proteinase K (Dako) for 10 min, the sections were incubated with the anti-VEGF primary antibody (mouse, Mab, clone C-1; Santa Cruz Biotechnology, Santa Cruz, CA) for 2 h at 37 °C. For endostatin immunostaining, following proteolytic digestion with protease (Protease XXIV, Sigma) for 10 min, the sections were incubated with the primary endostatin antibody (rabbit, polyclonal, Dianova GmbH, Hamburg, Germany) for 1 h at 37 °C. They were subsequently incubated with the linking biotinylated goat anti-mouse anti-rabbit secondary antibody (ChemMate Link, Biotinylated Secondary Antibodies, AB2, Dako), and with the streptavidin conjugated to alkaline phosphatase for 30 min each. Chromogen Red (ChemMate Detection Kit, Dako) was used as a chromogenic substrate. Levamisole was applied to inhibit endogenous alkaline phosphatase activity. Hematoxylin III according to Gill (Merck, Darmstadt, Germany) was used as a counterstain. For negative controls, the primary antibodies were substituted either by appropriate normal sera or omitted.

For better visualization of positive areas, donor eyes and CNV were examined after melanin bleaching. Melanin bleaching was performed according to the protocol established by Kivela (1995) and Makitie et al. (1998).

2.4. Analysis

Slides were analyzed by light microscopy. Intensity and presence of staining were determined three times independently by two masked observers (OT, SG) and the median score for each specimen was obtained. Inter- and intra-observer agreement was found in about 98% of the cases.

Based on the previous studies (Kvanta et al., 1996; Grossniklaus et al., 2002), the CNV membranes were classified as "inflammatory active (IA)" when inflammatory cells were more dominant than fibrosis (i.e. >50% inflammatory cells) or "inflammatory inactive (II)" when fibrosis was more dominant (<50% inflammatory cells) with minor or absent inflammatory response in CNV membranes.

Vascularization was evaluated by analyzing the specimens stained for CD34 and CD105 and counting the numbers of stained vessels in the most vascularized area under ×200 magnification. Every positive-staining endothelial cell or cell cluster that was separate from other vessels was counted irrespective of the staining intensity or the presence of a vascular lumen.

All Ki-67 positive nuclei in RPE, EC and stromal cells were counted separately in each specimen. The percentages of the Ki-67 expressing RPE, EC and stromal cells with regard to the total number of proliferating cells were determined. Proliferative activity (nuclei/mm^2) of a membrane was defined as the number of Ki-67 expressing nuclei in 1 mm^2 area of a specimen. Proliferative activity in each specimen was determined quantitatively by calculating the ratio of the total number of Ki-67 positive nuclei in CNV to the area of the membrane (mm^2).

Immunoreactivity for VEGF, endostatin and E-selectin was analyzed separately in RPE-Bruch's membrane complex, vessels and stroma. A grading scheme indicating the degree of staining was used. The values 3, 2, 1, 0 were assigned to indicate intense (70–100% positive cells), moderate (40–69% positive cells), weak labelling (1– 39% positive cells) and absence (–) of any staining, respectively. An "endostatin overall staining score", "E-selectin overall staining score" and "VEGF overall staining score" (range 0–9) was assigned to each membrane by summing up the staining scores in the three structures (RPE, stroma, EC) evaluated separately.

Statistics for the evaluation of proliferative activity and staining scores in the defined subgroups was performed with Mann–Whitney U test due to high variability of specimens. For correlation analysis, Spearman's correlation test was used; $p \leq 0.05$ was considered significant.

3. Results

3.1. Histologic characterization of control eyes

Six of the donor eyes ($n = 7$) were normal eyes without any ocular pathology, especially those associated with angiogenesis. One of the seven control eyes, however, disclosed drusen and sub-RPE deposits but no neovascularization. Demographic features and the immunohistologic findings of the control eyes are shown in Table 1 and Fig. 1, respectively.

For a better visualization and evaluation of the immunoreactivity within the choroid-Bruch's membrane-RPE complex, the melanin pigment was bleached. The staining pattern did not change after bleaching. Choroidal vessels displayed endostatin in 5 of 6 normal control eyes (Fig. 1A). Most of the choroidal vessels were endostatin positive in four of these

Table 1
Demographic features of the control eyes

Control eye	Age, sex	Eye	AMD
1	39, f	Right	–
2	62, m	Right	–
3	43, m	Right	–
4	52, f	Left	–
5	39, f	Left	–
6	49, f	Left	–
7	59, f	Right	+

AMD, age-related macular degeneration; f, female; m, male.

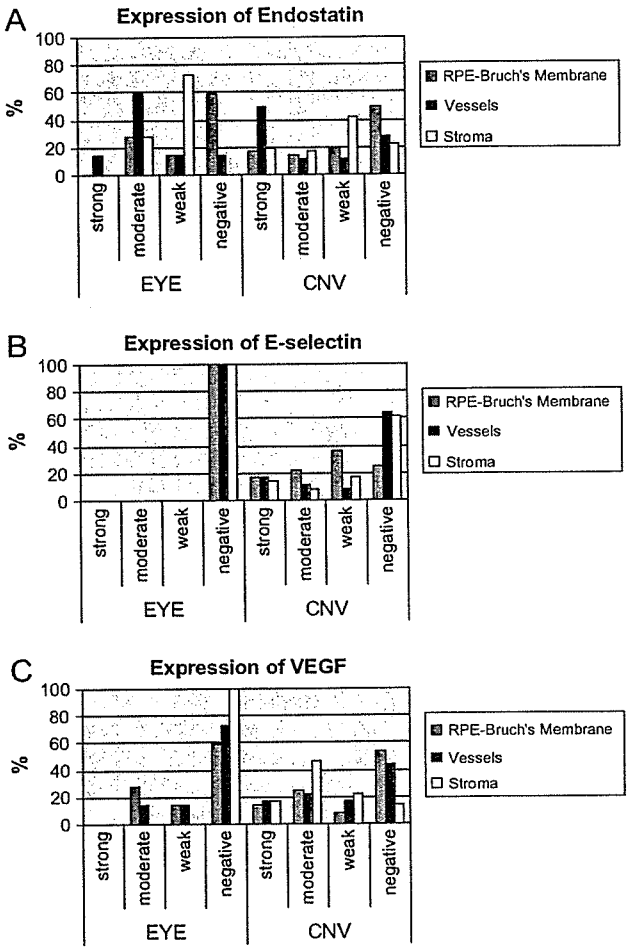

Fig. 1. Immunohistopathologic characteristics of the control eyes and CNV by analysis of the specimens for endostatin (A), E-selectin (B), and VEGF (C) separately in RPE-Bruch's membrane complex, vessels and stroma. For semi-quantitative evaluation, a grading scheme was used indicating the degree of staining: "strong" (70–100% positive cells); "moderate" (40–69% positive cells); "weak" (1–39% positive cells), "negative" (no positive cells).

eyes whereas in one eye only a few of the vessels expressed endostatin (Fig. 2A). The negative control of the same specimen by omitting the primary endostatin antibody displayed no staining in any of the structures (Fig. 2B). Endostatin staining was not specific to vessels. In 2 of 6 control eyes, RPE cells and Bruch's membrane were also stained for endostatin (Figs. 1A and 2C). Endostatin was not diffusely stained throughout a specimen as some endostatin expressing vessels (Fig. 2A) and RPE-Bruch's membrane complex (Fig. 2C) are detected beside the endostatin negative ones in the same specimen (Fig. 2A,D). Endostatin expression and variability in its pattern may be due to the local activity of the proteases in the setting which cleave only some of the endostatin from collagen XVIII. The absence of endostatin expression in RPE-Bruch's membrane complex in four of the control donor eyes (age range 39–62) leads us to assume that this commercial endostatin antibody detects only the free (cleaved) but not the bound form of endostatin. Staining for endostatin in varying intensities was seen in the choroidal stroma of all eyes. In the eye with drusen, endostatin expression was found in RPE-Bruch's membrane complex, stroma and choroidal vessels.

We next sought to investigate the expression of E-selectin and VEGF in the choroid. We found that none of the control eyes displayed E-selectin at all (Figs. 1B and 2E). In contrast, VEGF expression was present but still weak. RPE cells expressed VEGF moderately in two of the eyes. Weak to moderate expression of VEGF in choroidal vessels was also detected only in two eyes (Figs. 1C and 2F).

3.2. Histologic characterization of the CNV

All but one CNV were vascularized as evidenced by CD34 positive vessels. CD105 staining was specific to EC (Fig. 3A). CD105 was expressed in all the vascularized specimens ($n = 35$) to some extent (Fig. 3A). Within 13 of 35 vascularized CNV membranes (37%), some vascular ECs positive for CD34 did not express CD105. Contrary to control eyes, E-selectin was detected in RPE-Bruch's membrane, EC and some stromal cells in 75%, 36%, and 39% of CNV, respectively (Figs. 1B and 3B–D). Some CD34 positive EC as well as some RPE cells did not express E-selectin (Fig. 3B–D). CD 105 expressing EC were not always E-selectin positive (Fig. 3A,B).

Hematoxylin–eosin and PAS staining (Fig. 4A) were performed to determine the histologic orientation and to confirm the location of the diffuse drusen.

CK18 expressing RPE cells were found to be present in all of the CNV samples (Fig. 4B).

Positive staining for endostatin in RPE-Bruch's membrane was found in 50% of the membranes at varying intensities (Figs. 1A and 4C). In some CNV, endostatin expression was not evenly distributed in the RPE cell layer but was only partially expressed. Positive immunostaining in vessels was observed in 72% of the specimens (Figs. 1A and 4C–F). Endostatin staining in CNV specimens also persisted after bleaching of the specimen for melanin (Fig. 4D). Vessels in a CNV were only partially stained for endostatin (Fig. 4E). A few vessels expressing CD105 but no endostatin were detected. Endostatin expressing vessels were not always E-selectin positive (Figs. 3B and 4E). Staining intensity between vessels in the same CNV also varied. Endostatin staining was also observed in stromal cells and in fibrous stroma itself (Fig. 4F).

Endostatin and E-selectin were co-expressed in many CNV specimens (Figs. 3C,D and 4C,D). However, expression of endostatin in RPE-Bruch's membrane, vessels and stroma evaluated separately or as "the overall expression score" were not correlated with the corresponding E-selectin expression in CNV membranes ($p = 0.3482$, $\rho = 0.3130$; $p = 0.6294$, $\rho = -0.1610$; $p = 0.5658$, $\rho = -0.1820$; $p = 0.3978$, $\rho = -0.2670$, respectively)

In CNV, VEGF staining was absent in RPE cells of 53% of the specimens. When expressed, VEGF staining intensity in RPE varied from weak to strong. Similarly, VEGF expression in EC was seen in 55% of the CNV. Weak to moderate expression was found in 17% and 28% of the examined membranes, respectively. In 86% of the cases, VEGF expression could be

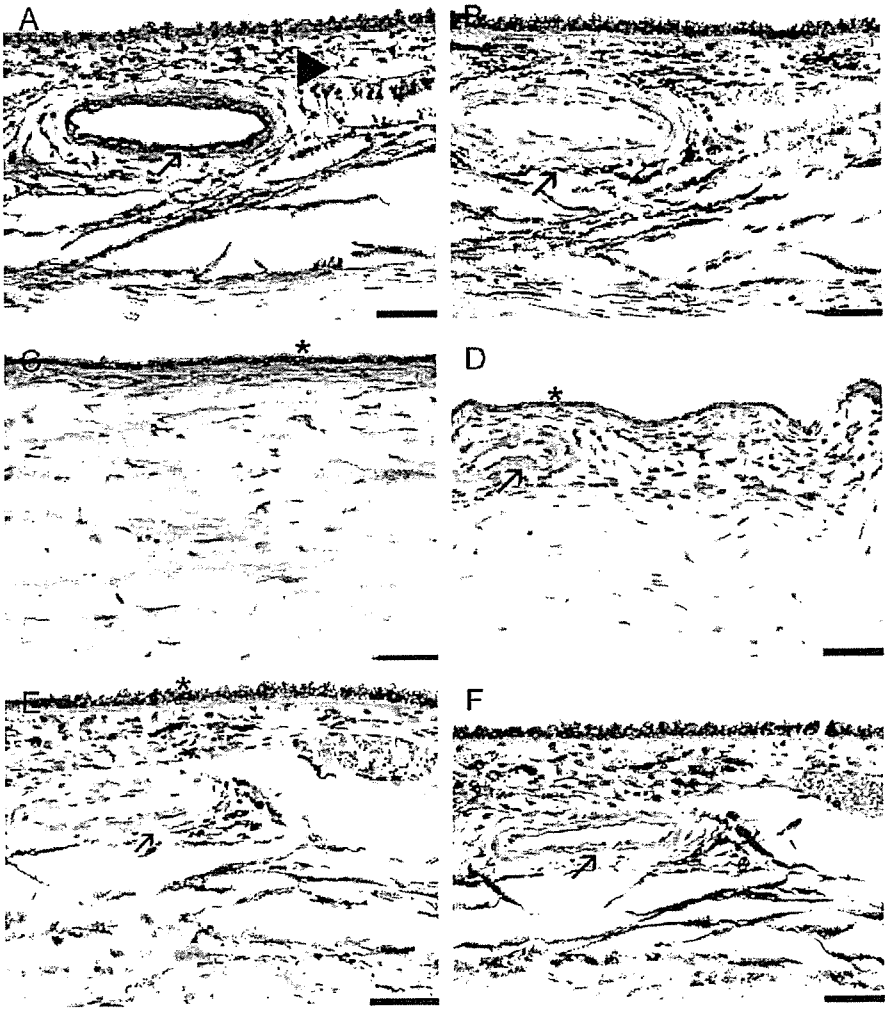

Fig. 2. Immunohistochemistry of a control eye (Case 4 in Table 1) probed with an antibody against endostatin (A, C, D), E-selectin (E) and VEGF (F). Sections were stained with either red alkaline phosphatase substrate (A–D, F) or AEC chromogen (E) and counterstained with hematoxylin. (A) Some vessels within the choroid disclose a prominent staining (arrow) whereas others are completely negative (arrowhead). (B) A serial section from the same specimen is used as a negative control by omitting the primary antibody "endostatin". None of the choroidal structures display false positive staining. (C) Endostatin labelling is present in part of the RPE-Bruch's membrane complex (*) whereas endostatin negative RPE-Bruch's membrane complex is also seen in the same eye (D, *). (D) A weakly stained choroidal vessel is apparent in the same section (arrow). (E) E-selectin is not expressed in any of the structures of the same eye (*:RPE, arrow:vessel) whereas VEGF is expressed weakly in some of the choroidal vessels (F, arrow). Scale bar: 50 μm.

encountered within the stroma of the membranes, especially in fibroblast-like and inflammatory cells (Figs. 1C and 5A). CNV membranes and vessels strongly stained both for VEGF and endostatin were also present (Figs. 4F and 5A).

3.3. Ki-67 labelling, proliferative and inflammatory activity in CNV

In CNV, a differing number of Ki-67 positive proliferating cells were detected. Ki-67 positive cells ($n = 971$) was rarely EC ($n = 51$, 5.3%) or RPE cells ($n = 36$, 3.7%) but mostly appeared to belong to stromal cells ($n = 874$, 90%), especially inflammatory infiltrate (Fig. 5B).

Proliferative activity in CNV membranes varied strongly from 0 to 514.01 nuclei/mm^2 (median 55.13, mean 105.72, SE 24.71). When "overall endostatin staining score" was concerned, there was no statistically significant difference in the median proliferative activity between the group with the high endostatin staining score (median 59.7, SE 31.67 overall, endostatin score 5–9, $n = 18$) and with the lower one (median 43.3, SE 38.88, overall endostatin staining score <5, $n = 18$) ($p = 0.4961$). High proliferative activity was observed in some CNV with strong endostatin expression (Figs. 4F and 5B). No correlation was found between the proliferative activity and the overall endostatin staining by Spearman's coefficient correlation test ($p = 0.321$, $\rho = 0.159$). Proliferative activity was also not correlated with either "E-selectin overall staining score" ($p = 0.622$, $\rho = 0.092$) or "VEGF overall staining score" ($p = 0.659$, $\rho = -0.075$).

Of the 36 CNV, 64% (23/36) was classified as inflammatory active (IA) whereas 36% (13/36) of the specimens were inflammatory inactive (II). There was no statistically significant